UCRL-JRNL-221813

Modelling the Pan-Spectral Energy Distribution of Starburst Galaxies: III. Emission Line Diagnostics of Ensembles of H II Regions

M. A. Dopita, J. Fischera, R. S. Sutherland, L. J. Kewley, C. Leitherer, R. J. Tuffs, C. C. Popescu, W. van Breugel, B. A. Groves

June 3, 2006

The Astrophysical Journal Supplement

Disclaimer

Modelling the Pan-Spectral Energy Distribution of Starburst Galaxies: III. Emission Line Diagnostics of Ensembles of H II Regions

Michael A. Dopita, Jörg Fischera, & Ralph S. Sutherland

Research School of Astronomy & Astrophysics, The Australian National University, Cotter Road, Weston Creek, ACT 2611, Australia

Lisa J. Kewley,

University of Hawaii at Manoa, Institute for Astronomy, 2680 Woodlawn Drive, Honolulu, HI 96822, USA

Claus Leitherer

Space Telescope Science Institute, 3700 San Martin Drive, Baltimore MD21218, USA

Richard J. Tuffs, Cristina C. Popescu,

Max-Plank-Institut für Kernphysik, Saupfercheckweg 1, D-69117 Heidelberg, Germany

Wil van Breugel

Institute of Geophysics and Planetary Physics, Lawrence Livermore National Laboratory, L-413 Livermore, CA 94550, USA

& Brent A. Groves

Max-Plank Instute for Astrphysics, Karl-Schwartzschild-Str 1, 85741, Garching, Germany

Michael.Dopita@anu.edu.au

ABSTRACT

We have built, as far as possible, fully self-consistent models of H II regions around aging clusters of stars. These produce strong emission line diagnostics applicable to either individual H II regions in galaxies, or to the integrated emission line spectra of disk or starburst galaxies. The models assume that the expansion and internal pressure of individual H II regions is driven by the net input of mechanical energy from the central cluster, be it through winds or supernova events. This eliminates the ionization parameter as a free variable, replacing it with a parameter which depends on the ratio of the cluster mass to the pressure in the surrounding interstellar medium. These models explain why H II regions with low abundances have high excitation, and demonstrate that at least part of the warm ionized medium is the result of overlapping faint, old, large, and low pressure H II regions. We present a number of line ratios (at both optical and IR wavelengths) that provide reliable abundance diagnostics for either single H II regions or for integrated galaxy spectra, and others that are sensitive to the age of the cluster stars exciting individual H II regions.

Subject headings: galaxies: general – galaxies: star formation rates – galaxies: abundances – galaxies: starburst –ISM: H II –ISM: abundances-

1. Introduction

Much of what we have learnt about the chemical evolution of the Universe, or of individual galaxies throughout cosmic time has been gleaned from the study of the spatially unresolved and therefore integrated emission line spectra of distant disk or starburst galaxies (Steidel et al. 1996; Kobulnicky, Kennicutt & Pizagno 1999,?; Kewley & Kobulnicky 2005). This emission line spectrum arises from the ensemble of H II regions within the galaxy, and these are characterized by a wide range of physical parameters.

For example, in disk galaxies, the chemical abundance of heavy elements falls continuously from centre to edge. In like manner, the pressure and density of the interstellar medium in the disk drops exponentially with radius. For a given input of mechanical energy by the central star cluster, this means that the outermost H II regions expand more rapidly, and will therefore be both larger and with lower internal pressure at a given age. However, the properties of the central cluster of a given mass change systematically with chemical abundance. Massive stars with higher chemical abundances lose more mass prior to supernova explosion, have stronger stellar winds, evolve more rapidly, and have lower effective temperatures while on the Main Sequence.

Finally, the temporal evolution of individual H II regions is extremely important in determining the integrated emission line spectrum. Leitherer, Gruenwald & Schmutz (1992) demonstrated just how important aging of the OB stars is in lowering the number of ionizing photons as the most massive stars evolve away from the Zero Age Main Sequence (ZAMS) to become supergiants. Later, these stars have a brief resurgence in their ionizing photon and mechanical energy production as they become Wolf-Rayet stars.

With so many temporal and physical variables, it is perhaps not surprising that the nebular modelling community (ourselves included) have in the past been reduced to making severe, even gross, oversimplifications in attempts to model the integrated strong emission line spectra of galaxies. Indeed, often only a single line ratio has been used to determine the metallicity of extragalactic H II regions or even of whole galaxies. This is the famous R_{23} ratio; ([O II] λ3727 + [O III] $\lambda\lambda$4959,5007)/Hβ.

The use of this ratio was first proposed by Pagel et al. (1979). The logic for the use of this ratio is impeccable, since it uses the two strongest lines of the strongest coolant of H II regions, and it should therefore be sensitive to the total oxygen abundance. By using two stages of ionization, it accounts for the emission in the bulk of the ionized nebular volume. However, the calibration of this ratio in terms of the abundance has proved to be rather difficult and many calibrations of R_{23} are available, including Pagel et al. (1979); Pagel, Edmunds & Smith (1980); Edmunds & Pagel (1984); McCall, Rybski & Shields (85); Dopita & Evans (1986); Torres-Peimbert, Peimbert & Fierro (1989); Skillman, Kennicutt & Hodge (1989); McGaugh (1991); Zaritsky, Kennicutt & Huchra (1994); Pilyugin (2000); Kewley et al. (2002b),

The reason for the difficulty in calibrating the R_{23} ratio is common to many ratios formed from the flux of optical forbidden line divided by the flux of a recombination line of hydrogen. Initially, as Z is increased, the forbidden line increases in flux, and the line ratio increases. However, as the abundance increases further, the cooling by forbidden lines lowers the electron temperature making it more difficult to collisionally excite the optical forbidden lines. Eventually there comes a point at which an increase in abundance is matched by a decrease in collisional excitation and the line ratio reaches its maximum. Any further increase in Z then leads to a *decrease* in the relative strength of the forbidden line. R_{23}, like other optical diagnostics is therefore a two-valued function of Z. Because infrared lines have lower thresholds for collisional excitation, they remain monatonic functions of Z up to much higher metallicities. Recognizing this physics, the S_{23} ratio; ([S II] $\lambda\lambda$6717,31 + [S III] $\lambda\lambda$9069,9532)/Hβ has been used more recently in the place of, or to supplement the R_{23} ratio (Dennefeld & Stasinska 1983; Kennicutt & Garnett 1996; Oey et al. 2000).

Moving beyond the use of single line ratios, further sophistication is possible relying on the understanding that the strong line emission spectrum of an individual H II region is controlled by three physical parameters (Dopita & Evans 1986). These parameters are, the effective temperature of the exciting stars, the chemical abundance set (or "metallicity", Z) and the ionization parameter, defined either as the ratio of the mean ionizing photon flux to the mean atom density, q or in its dimensionless form as the ratio of mean photon density to mean atom density $\mathcal{U} = q/c$. Thus, for a given stellar input spectrum a $\mathcal{U} : Z$ grid of models will provide the ideal means of interpreting the observational data (Kewley et al. 2002b).

This leaves open the question of the age distribution of the exciting stars, which together with the metallicity determines the energy distribution of the EUV photons. In the modelling hitherto, this problem is usually treated in two limits; the instantaneous burst approximation (for which zero age is often, but not universally assumed) or the continuous star formation approximation in which stars are assumed to be born continually within the ionized region (see Kewley et al. (2001), and references therein). All this modeling effectively assumes a single H II region of a given metallicity and ionization parameter. Whilst such an approach is acceptable in attempts to understand the emission line spectrum of individual H II regions, it is certainly inadequate in attempts to interpret the integrated spectrum of a whole galaxy, or even of a complex of many H II regions.

The advent of the *Starburst 99 v.5* (Leitherer et al. 1999) stellar spectral synthesis code finally allowed the construction of fully self-consistent models for H II regions. For a given stellar initial mass function (IMF), this code delivers not only the pan-spectral distribution of photons, including ionizing photons as a function of age, but also provides tables of the time-dependent mechanical energy input of the stars including OB-star stellar winds, red giant winds, Wolf-Rayet winds and the energy input from supernova explosions.

In the first paper of this series (Dopita et al. (2005), hereinafter referred to as Paper I), we computed the (one dimensional) evolution of H II regions around clusters of a single mass to demonstrate how the size : age relation is essentially determined by the density (or pressure) in the surrounding interstellar medium (ISM). This in turn determines the dust 'temperature' described by the wavelength of the peak of the far-IR dust re-emission feature.

In the second paper (Dopita et al. (2006), in press, hereinafter referred to as Paper II), we investigated the role of metallicity and of the cluster mass function in controlling the excitation of the populations of H II regions in galaxies, be they disk or starburst. In particular, we showed that the ionization parameter is controlled by the cluster mass, the pressure in the surrounding ISM and the metallicity and age of the exciting cluster. This allowed us to compute the probability distributions of H II region ionization parameters in galaxies as a function of metallicity and pressure in the ISM.

With these insights, we can now proceed to the next stage of sophistication in modeling – the construction of ensemble averages of aging H II regions. In this paper we will investigate the emission line diagnostics of such ensembles of H II regions in galaxies with the view to assisting the optical or IR analysis of the strong line emission lines of both individual H II regions and of more distant and unresolved galaxies. Such analyses allow us to derive star formation rates, estimate metallicities, and infer ages for individual H II regions.

2. Models

2.1. Codes

We have used the *Starburst 99 v.5* code in its latest (2005) version to compute the pan-spectral distribution of clusters of stars with a piece-wise fit to a Miller-Scalo initial mass function (IMF) Miller & Scalo (1979) between 0.1 and 120 $M_{\odot}$. The parameters of this fit are the same as given in Miller & Scalo (1979) and were also tabulated by us in Paper II. Either the use of a Miller-Scalo IMF or of a Salpeter IMF would not noticeably affect the line ratio diagnostics presented in this paper, since the slopes of the IMF are almost identical above 10 $M_{\odot}$. However, the choice of the IMF has a much larger effect on the total mass of the cluster, since this is determined by the choice of the power law below 10 $M_{\odot}$.

Stellar atmosphere models for stars with plane parallel atmospheres are based on the Kurucz (1992) models as compiled by Lejeune (1997). The fully line-blanketed Wolf-Rayet atmosphere models of Hillier & Miller (1998) and the non-LTE O-star atmospheres of Pauldrach, Hoffman, & Lennon (2001) have been incorporated into *Starburst 99 v.5* as described in Smith, Norris & Crowther (2002).

For a given cluster mass, we used the stellar wind and supernova power output, as tabulated by the *Starburst 99 v.5* code, to solve for the radius of the H II regions as a function of time given the pressure or, equivalently, the mean density in the ISM. This requires a Runge-Kutta integration of the equation of motion of the swept-up shell, as was done and described in both Paper I and Paper II.

The pressure in the H II region is the same as in the shocked stellar wind gas. This is given by the classical Castor, McCray (1975) theory;

$$P(t) = \frac{7}{(3850\pi)^{2/5}} \left(\frac{250}{308\pi}\right)^{4/15} \left(\frac{L_{\rm mech}(t)}{\mu m_H n}\right)^{2/3} \frac{\mu m_H n_0}{r(t)^{4/3}} \qquad (1)$$

where $L_{\rm mech}(t)$ is the instantaneous production of mechanical energy by the cluster stars, $r(t)$ is the radius, n_0 is the mean atom density in the surrounding ISM and n is the mean atom density in the ionized gas.

In Paper II, we showed that the ionization parameter at the contact discontinuity in the swept-up shell of ISM, which can be treated as the inner boundary of the H II region depends largely on the instantaneous properties of the exciting cluster stars;

$$q(t) \propto \delta(t)^{3/2} S_*(t)/L_{\rm mech}(t). \qquad (2)$$

where $S_*(t)$ is the instantaneous flux of ionizing photons from the central cluster.

The presence of the $\delta(t)$ factor in the above equation provides a weak coupling between the ionization parameter and both the pressure in the ISM, P_0, and the mass of the central cluster, M_{cl}. Together, these determine the strength of the outer shock of the mass-loss bubble and therefore the compression factor through it. The appropriate scaling factors are $q \propto P_0^{-1/5}$ and $q \propto M_{cl}^{1/5}$. Thus, once P_0 and $q \propto M_{cl}^{1/5}$ are fixed, the ionization parameter is determined.

Finally, the latest version of our code *Mappings IIIr* (Sutherland & Dopita 1993; Dopita et al. 2002; Groves, Dopita & Sutherland 2004) and Paper I was used to compute photoionization models the isobaric dusty H II with these parameters to produce a table of emission lines which are subsequently used in the line ratio diagnostics described in this paper.

2.2. Metallicities & Depletion Factors

The solar abundance set is taken from Asplund, Grevesse & Sauval (2005), which incorporates the results of many papers which together have provided a self-consistent recalibration of the solar abundance. In general, these abundances are nearly a factor of two lower than those used previously (Anders & Grevesse 1989).

The depletion factors from the gaseous phase determine the composition of the dust in the models. For these we have took the measured gas-phase abundances in the local interstellar cloud by Kimura, Mann & Jessberger (2003), and used these to infer a set of local depletion factors consistent with the Asplund, Grevesse & Sauval (2005) abundance set. The resulting solar abundances (given as log A/H and the adopted depletion set is given in table 1. For models with non-solar abundances, the depletion factors were held constant at solar values, equivalent to taking the dust : gas ratio to be proportional to metallicity.

Three elements do not scale simply with the metallicity. First, because of its high initial abundance as a result of nuclear burning in the Big Bang, Helium scales only weakly with metallicity. For this element, we assume a primary nucleosynthesis component in addition to its primordial value. From Russell & Dopita (1992) and Pagel et al. (1992) we infer the empirical relationship:

$$\mathrm{He/H} = 0.0737 + 0.024 \times \mathrm{Z/Z_{\odot}}. \tag{3}$$

For both Nitrogen and Carbon there is clear evidence that these are both a primary nucleosynthetic element, dominant at low metallicity, and a secondary nucleosynthetic element once higher abundances are reached. Alternatively, both are produced in part by dredge-up in intermediate mass stars, causing a delay in the onset of enrichment of these elements from this source. For Nitrogen we have used a modified version of the form proposed by Groves,

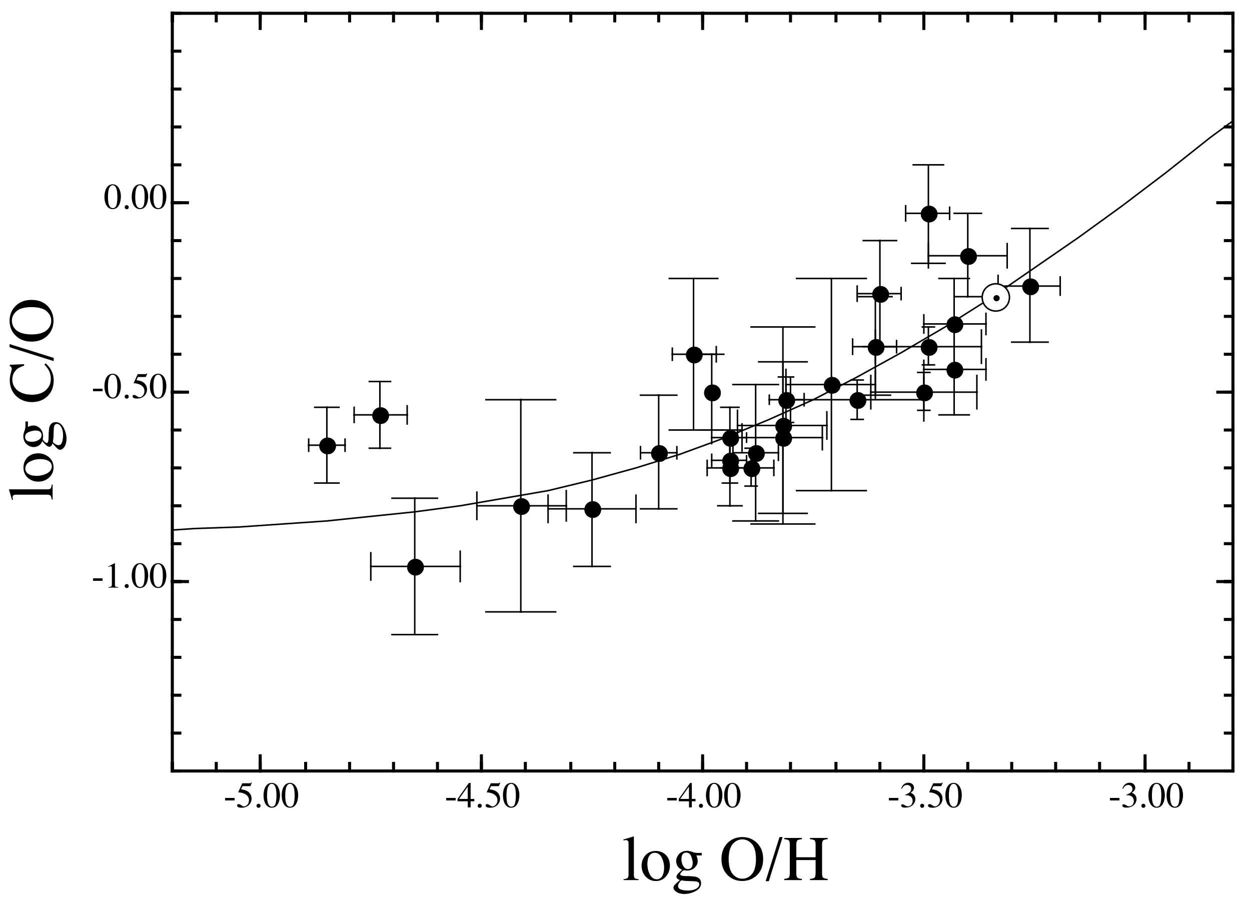

Fig. 1.— The fit given by equation 5 is shown along with the HST observations of H II regions made by Garnett et al. (1999). The solar abundance from Asplund, Grevesse & Sauval (2005) is also marked with an $\odot$ symbol. The new solar abundance set eliminates the systematic difference between the solar and the H II region abundances noted by Garnett et al. (1999)

Dopita & Sutherland (2004);

$$\mathrm{N/H} = 1.1 \times 10^{-5} Z/Z_{\odot} + 4.9 \times 10^{-5} Z/Z_{\odot}{}^{2}. \tag{4}$$

For Carbon, we have used the HST data on the Carbon abundances of H II regions as compiled by Garnett et al. (1999). This provides a fit of the same mathematical form as for N:

$$\mathrm{C/H} = 6.0 \times 10^{-5} Z/Z_{\odot} + 2.0 \times 10^{-4} Z/Z_{\odot}{}^{2}. \tag{5}$$

The fit to the observations is shown in figure 1.

2.3. Parameters of the Models

The *Starburst 99 v.5* code allows us to study line ratios at five (fixed) metallicities, $Z/Z_{\odot} = 0.05, 0.2, 0.4, 1.0$ and 2.0. For each of these abundance sets we have computed several families of H II region models with ages 0.2, 0.5, and 1.0 Myr and in further 0.5 Myr steps up to 6.0 Myr. By this time, more than 94% of ionizing photons have been emitted, the H II regions have faded by factors of between 5 and 12 from their peak luminosity, and their surface brightnesses will have faded by much greater factors than these.

As described above, at any age t, the instantaneous ionization parameter, which determines the excitation of the H II region is governed by the ratio of the mass of the cluster and the pressure in the surrounding ISM. We therefore define a quantity $R = (M_{\mathrm{cl}}/M_{\odot})/(P_0/k)$, where P_0/k is measured in cgs units; cm^{-3}K. Since cluster masses may vary between $\sim 100 M_{\odot}$ and $10^5 M_{\odot}$, and the likely range of ISM pressures are between $10^3 < P_0/k < 10^7$ cm^{-3}K then reasonable values for R fall within the range $-6 < \log R < +2$. We have therefore computed, for each metallicity and age, H II regions having $\log R = -6, -4, -2, 0$ and $+2$. For a given metallicity, the instantaneous value of the ionization parameter depends on $R^{1/5}$, as we have shown in Paper II.

Together, the parameters $Z/Z_{\odot}, t$ and $\log R$ define a unique H II region spectrum, with one caveat, namely, that if the density of the ionized gas becomes too high, then collisional de-excitations of forbidden lines will alter the emergent spectrum. This only becomes a concern at the very highest values of ISM pressure either within ultra-compact H II regions (as computed by Dopita et al. (2006) or else in starburst environments with $P_0/k > 10^7$ cm^{-3}K. For the current purposes, we have computed the particular case of $P_0/k = 10^6$ cm^{-3}K, which constrains the electron density in the H II region below $\sim 100\mathrm{cm}^{-3}$ except at very earliest times and in the models of highest metallicities, where it may reach $\sim 10^3\mathrm{cm}^{-3}$.

For each model, we have prepared tabular data for all the strong lines between the Lyman Limit and 88μm. For each $Z/Z_{\odot}$: $\log R$ age sequence, we have also formed Hβ flux weighted time averaged spectra to represent the integrated spectrum for a given $Z/Z_{\odot}$ and $\log R$. These spectra are available on-line, and the form of the tables is given in the Appendix.

3. H II Region emission Line Diagnostics

3.1. Optical Lines

3.1.1. Veilleux & Osterbrock Diagnostics

The diagnostics that have been most frequently used in the classification of the nature of nebular excitation are those proposed by Veilleux & Osterbrock (1987) (hereinafter V&O). The most popular of these is the [N II] λ6584/Hα *vs.* the [O III] λ5007/Hβ ratio, and in the other two [S II] $\lambda\lambda$7617,31/ Hα or [O I]λ6300/Hα are substituted in place of the [N II] λ6584/Hα ratio.

These V&O ratios have the virtue of only using lines which are close together in wavelength in forming the ratio, so errors due to uncertain reddening corrections are avoided. These plots also nicely separate H II regions from regions excited by active galactic nuclei (Seyfert or LINER nuclei) and from shock-excited objects. The H II regions form an extremely tight sequence, particularly in the diagram using the [N II] λ6584/Hα ratio.

The results of our modelling for the [N II] λ6584/Hα *vs.* the [O III]/Hβ ratio is shown in figure 1. Because of the difficulty of representing so many theoretical models on the same figure, this is presented here in color, and in four panels. The first panel shows models of all ages for each metallicity, color coded for clarity. The model series corresponding to $\log R = -2$ is drawn bold, since this is our best guess of the most likely value of $\log R$ in disk galaxies ($10^2 \leq M_{\rm cl}/M_{\odot} \leq 10^4$ and $10^4 \leq P/k \leq 10^6$ cm^{-3}K). The remaining three panels show the complete grid of models for $\log R = 0, -2$ and -4, respectively. Isochrones are plotted for 0.2, 1.0, 2.0, 3.0 and 4.0 Myr.

In this figure, as in the others we will present, the observational datasets for individual H II regions are presented as crosses, and integrated spectra of galaxies as dots. For the H II regions the data are drawn from van Zee et al. (1998); Kennicutt & Garnett (1996); Dennefeld & Stasinska (1983); Walsh & Roy (1997); Roy & Walsh (1997) and the extension of the data set to low abundances is from Pagel et al. (1992). The integrated galaxy spectroscopy comes from Moustakas & Kennicutt (2005) and Moustakas & Kennicutt (2006). There is

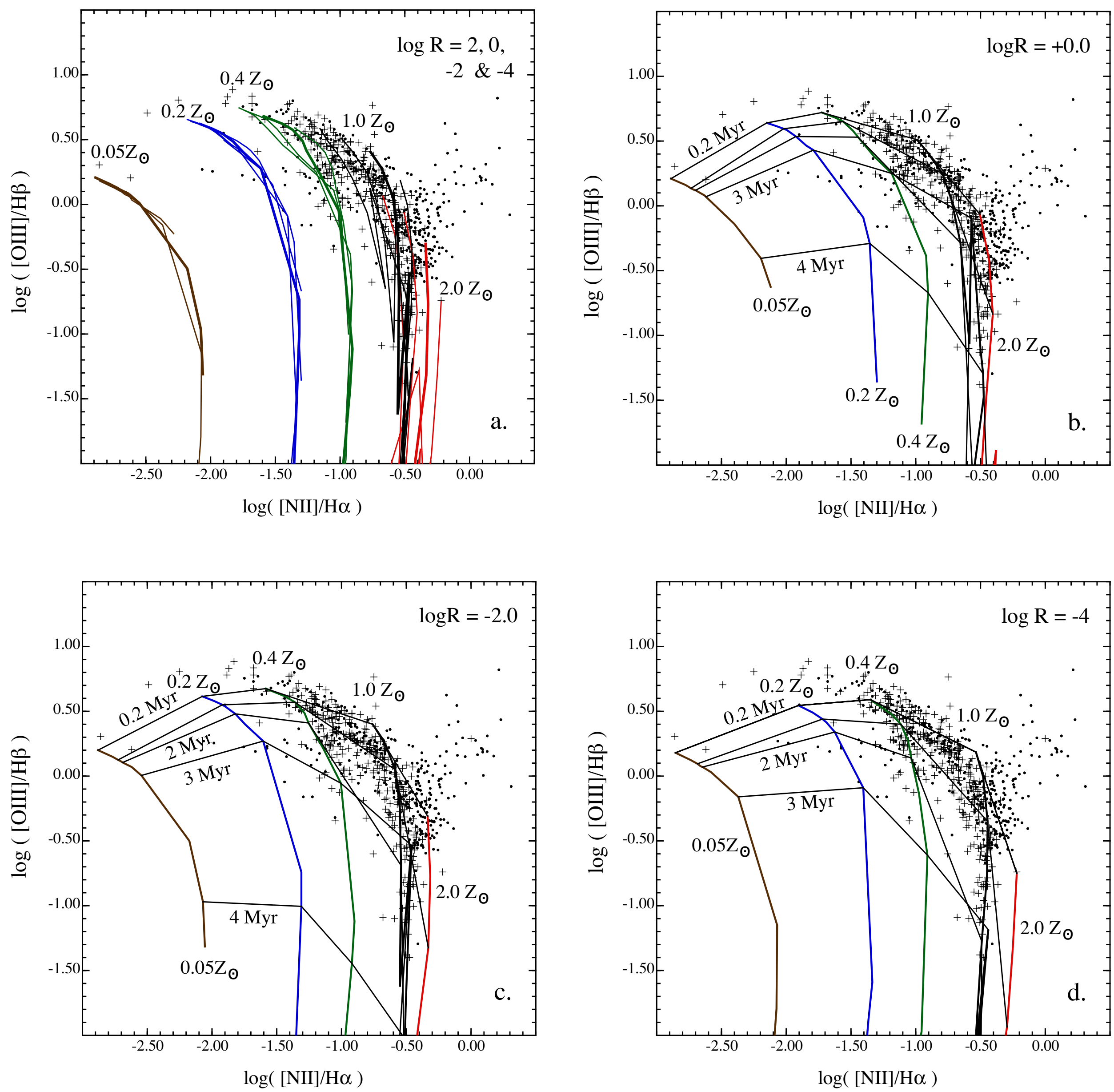

Fig. 2.— The [N II] $\lambda6584$/Hα *vs.* the [O III] $\lambda5007$/Hβ ratio. The abundances are coded by color; for $Z/Z_{\odot}0.05, 0.2, 0.4, 1.0$ and 2.0 the colors are brown, blue, green, black and red, respectively. Selected observational data sets for individual H II regions are marked as crosses, and integrated galaxy spectra from Moustakas & Kennicutt (2005) are shown as points. In panel (a) we plot all models of a given metallicity, and in the remaining panels we plot ageing tracks at each metallicity and the corresponding isochrones for three likely values of the R parameter; $\log R = 0, -2$ and -4, respectively.

some contamination of these latter points by the presence of Seyfert nuclei, which accounts for the spray of points to high values of the [N II]/Hα ratio, and to higher values of the [O III] λ5007/Hβ ratio. Overall, the integrated galaxy spectra tend to have larger and [N II]/Hα ratios and lower [O III]/Hβ ratios, although the distinction with individual H II region is not marked.

The reason why the observed H II regions on a [N II]/Hα *vs.* the [O III]/Hβ form such a narrow sequence is quite evident. First, to be bright, and therefore selected for observation, observed H II regions should have an age less than ~ 3 Myr. In this age range, the isochrones of all models of different abundances fall into the very narrow strip defined by the observations. Although it depends somewhat on the assumed value of $\log R$, it is clear that no observed H II region has an age greater than $3 - 4$ Myr, consistent with the presumption of strong observational selection against old H II regions.

This figure should be compared with Figure 2 of Dopita et al. (2000), in which a grid of models in $Z/Z_{\odot}$ and q, the ionization parameter were presented. It is clear that, in order to have a low metallicity H II region with a low ionization parameter, the H II region has to be faint and old, and would therefore not have been observed in these surveys. For metallicities greater than about $Z/Z_{\odot} \sim 0.5$, all models are highly degenerate in metallicity and age. It is this fact which accounts for the very tight distribution of observed points in the region of the plot where log([O III]/Hβ)< 0.0.

Since the models of Dopita et al. (2000) were run, the EUV field predicted by the *Starburst 99 v.5* code has softened, thanks to improvements in the treatment of extended atmospheres. This leads both to the reduction in the limiting [N II]/Hα ratio seen in figure 1, which improves the fit with the observations, and the decrease in the limiting [O III]/Hβ ratio, which tends to make the fit somewhat worse at the low metallicity end.

Note, particularly visible in panel (c) of figure 2, that the ageing tracks make a sharp zig-zag causing the 3 Myr isochrone to lie above the 4 Myr isochrone for metallicities above solar. This is the result of the Wolf-Rayet stars, which briefly harden the overall stellar radiation field before themselves exploding as Type II supernovae.

The fit between theory and observation is much less striking when we consider the second of the Veilleux & Osterbock diagrams which plots the [S II] $\lambda\lambda$7617,31/Hα ratio *vs.* the [O III] λ5007/Hβ ratio. This is shown in figure 3. In general, the predicted [S II] lines are weaker than observed, by as much as a factor of two. A similar effect was seen in our earlier modeling (see figure 3 of Dopita et al. (2000)).

The interpretation of the [S II] $\lambda\lambda$7617,31/Hα ratio is more confusing than the [N II] λ6584/Hα ratio if we wanted to use it as an abundance indicator, particularly at high metallicity. How-

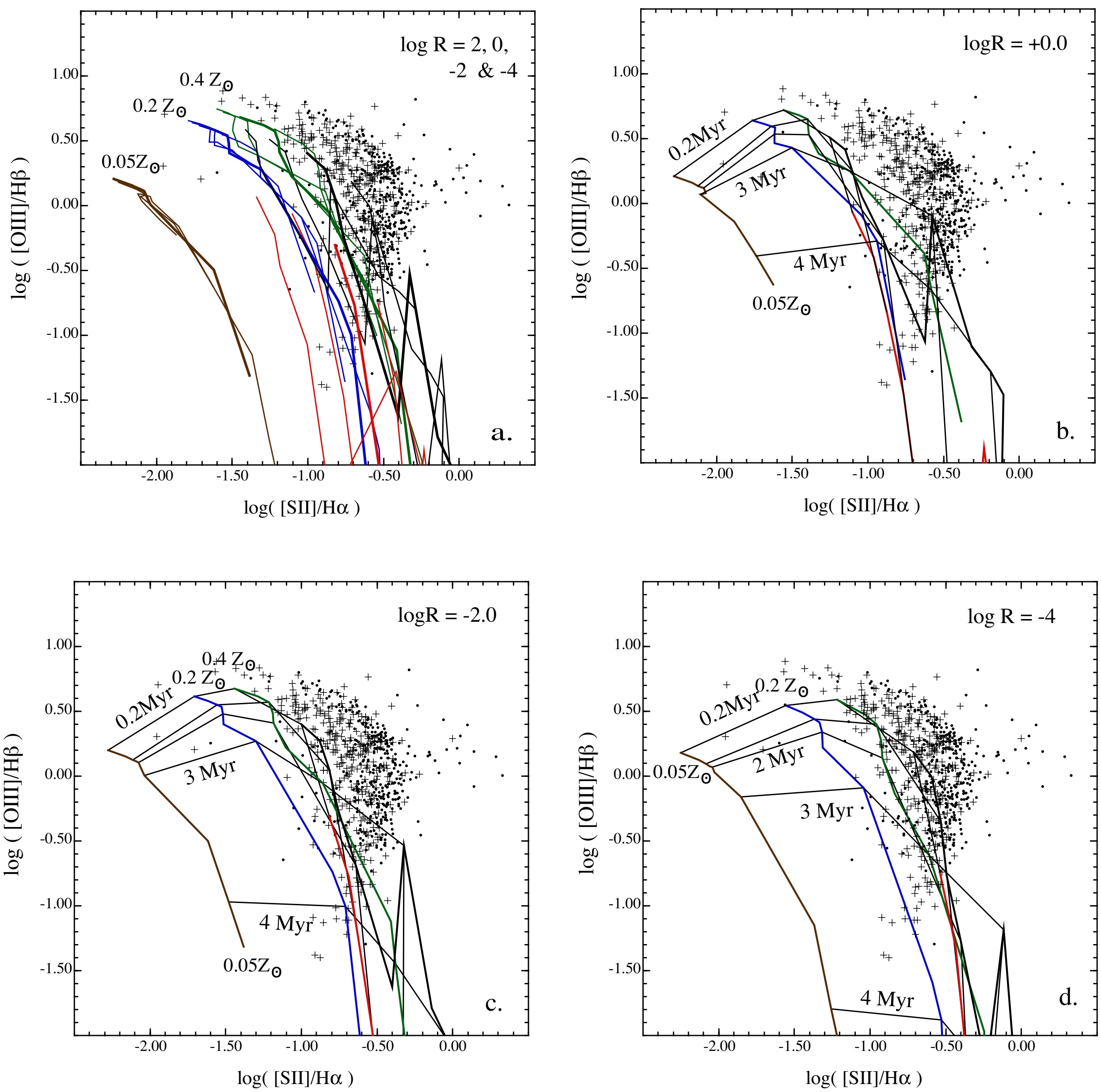

Fig. 3.— As figure 2 but for the second of the V&O diagnostics, the [S II] $\lambda\lambda$7617,31/Hα ratio *vs.* the [O III]/Hβ ratio.

ever, the 0.2 - 3 Myr isochrones still define a narrow range in line ratio space, albeit not exactly coincident with the observations. The reasons for such a discrepancy between theory and observation in this, as well as in other line ratio plots will be discussed in section 5.

3.1.2. The BPT Diagram

Baldwin, Phillips & Terlevich (1981) (BPT) first proposed the use of the [O III] λ5007/[O II] $\lambda\lambda$3727,29 vs the [O III] λ5007/Hβ ratio as a line diagnstic to separate active nuclei from H II regions and to provide an excitation sequence for H II regions. Our results for this line ratio are shown in figure 4.

The [O III]/[O II] ratio is a measure of the excitation of the nebula, and for a given input spectrum is therefore sensitive to the ionization parameter. Because they have higher ionization parameters and also have central stars with higher effective temperatures for a given age, the low-metallicity H II regions are characterized by higher [O III]/[O II] ratios. Like all other ratios of optical forbidden lines to recombination lines, for a given stellar age, the [O III] λ5007/Hβ ratio starts off low at low metallicity, reaches a maximum at a certain metallicity, and then declines swiftly at higher metallicities. The reason for this was explained in the introduction in the context of the R_{23} ratio. As a consequence, the BPT diagram is highly degenerate in metallicity in the range $0.2 \leq Z/Z_{\odot} \leq 2$, explaining the tightness of the observed H II region sequence. This means, however, that the [O III]/Hβ ratio is of little use as an abundance diagnostic except for $Z/Z_{\odot} \leq 0.2$, and even then it requires the [O III]/[O II] ratio to have also been determined for an Oxygen abundance to be derived from it.

Although the theoretical sequence has much the same form as defined by the observations, it is notable that, for all values of the [O III]/[O II] ratio, the maximum of the [O III]/Hβ lies below the maximum defined by the observations. Furthermore, even for the highest value of $\log R$, the zero-age models do not reach to the maximum [O III]/[O II] ratio defined by the observations. As discussed in section 5, below, both of these discrepancies can be ascribed to a single source, namely that the input spectrum we are using in the models is somewhat 'softer' than the EUV spectrum found in real H II regions.

3.1.3. The R_{23} *Ratio*

As described in the introduction, the R_{23} ratio has had a long history in various attempts to determine abundances using ratios of strong emission lines. Normally, one at-

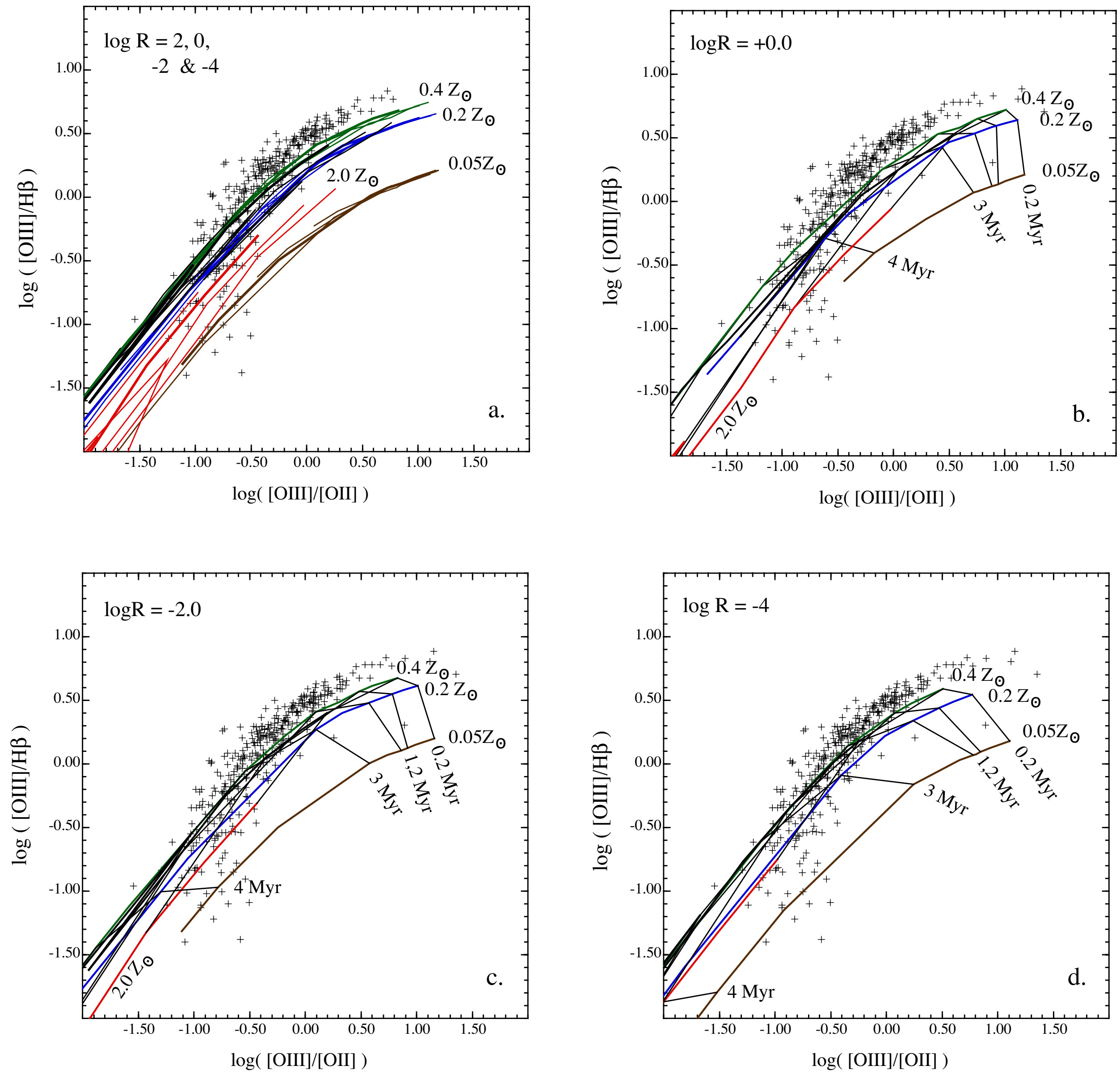

Fig. 4.— As figure 2 but for the [O III] λ5007/[O II] $\lambda\lambda$3727,29 vs the [O III] λ5007/Hβ ratio. This is the diagnostic first used by Baldwin, Phillips & Terlevich (1981) (BPT) to separate AGN from H II regions. To distinguish them visually, the low abundance H II regions from Pagel et al. (1992) are plotted only on panels (b) to (d). Note how these are concentrated on the upper right of the figure, and how the lowest metallicity points fall below the main sequence of observed H II regions. High metallicity H II regions ($Z/Z_{\odot} > 2$) are located in the lower right hand corner of this diagram.

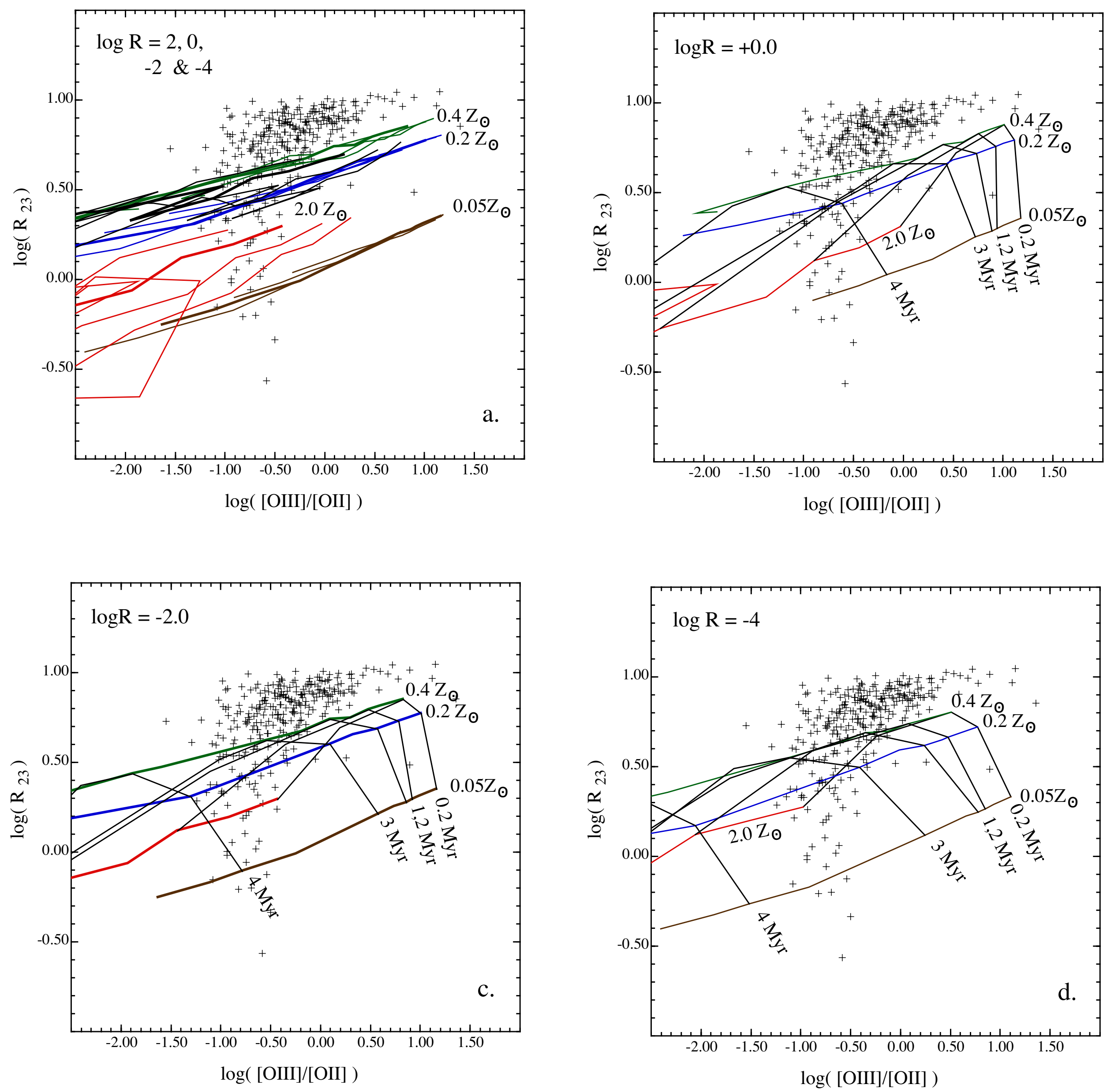

Fig. 5.— As figure 2 but for the R_{23}— ratio *vs.* the [O III] λ5007/[O II] $\lambda\lambda$3727,29 ratio. In panels (b) to (d) the solar metallicity track has been omitted for clarity. This shows that the traditional R_{23} ratio is not a good abundance diagnostic in the range $0.2 \leq Z/Z_{\odot} \leq 1.5$, approximately, and that it is quite sensitive to the nebular excitation. The theoretical tracks are, however, a rather poor fit to the observations. This is because the models have both [O III] $\lambda\lambda$4959,5007 and [O II] $\lambda\lambda$3727,29 weaker than those actually observed.

tempts to derive the metallicity directly from the R_{23} ratio. However, the sensitivity of the [O III] λ5007/Hβ ratio to the cluster age shown in figure 4 suggests that we should plot the R_{23} ratio against the [O III]/[O II] ratio in order to be able to investigate the age sensitivity of the R_{23} ratio. This diagnostic is shown in figure 5.

For this diagnostic the fit between theory and observation is quite poor, due mainly to the fact that the R_{23} ratio is systematically underestimated in the models. The size of the effect is larger than is seen in he [O III]/Hβ ratio (see figure 4), showing that predicted strengths of *both* the [O III] and the [O II] lines are too weak. If the theoretical curves could be shifted upwards, and to the right, then the fit to observation would be much better. How such a shift could be accomplished is discussed in Section 5.

The form of the theoretical tracks on this diagnostic plot shows immediately why the calibration of the R_{23} ratio in terms of metallicity has been so difficult. Not only is the range of R_{23} rather restricted, but is it degenerate in terms of metallicity over a rather generous range, $0.2 \leq Z/Z_{\odot} \leq 1.5$, approximately. Not only that, but the ratio is fairly sensitive to excitation, as measured by the [O III]/[O II] ratio. Because low metallicity H II regions are characterized by high ionization parameters, the low metallicity points tend to occur in the upper right of this plot, while the spray of points towards the bottom left of this diagnostic can only be due to very high metallicity H II regions with ages of 1–3 Myr.

Based on these problems, we are constrained to conclude that R_{23} is not a good abundance diagnostic. We will return to this point in Section 5, below.

3.1.4. Dopita et al. (2000) Diagnostics

Dopita et al. (2000) introduced two new abundance diagnostics, based on the [N II]/[O II] line ratio. This ratio was favoured for two reasons which make it *very* sensitive to abundance. The first is that, over much of the range of interest, nitrogen is a secondary nucleosynthesis element, or at least has a large secondary component. Thus the ratio [N II]/[O II] will systematically increase with abundance. The second is connected with the fact that the [O II] $\lambda\lambda$3727,29 lines are found in the near UV part of the spectrum, whereas the [N II] λ6584 is in the red part of the spectrum. This might be construed as a disadvantage in the use of the [N II]/[O II] ratio, since the reddening corrections are large, and correspondingly more uncertain. However, this problem is more than offset by the fact that the mean temperatures of H II regions are a strongly decreasing function of metallicity and at high abundances, the mean thermal energy of the electrons becomes too low to excite transitions with large electron excitation energy. Thus transitions such as the [O II] $\lambda\lambda$3727,29 lines

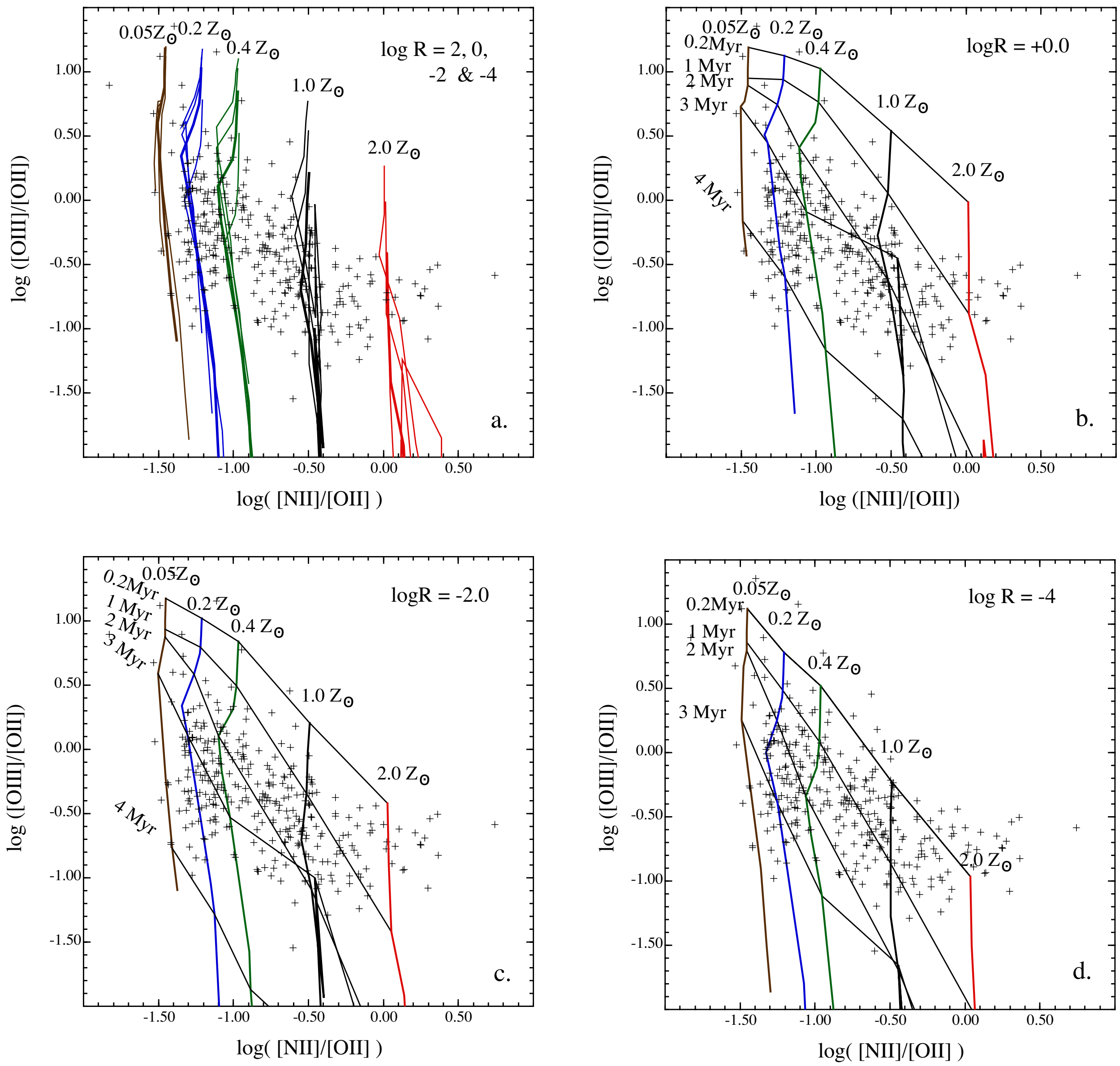

Fig. 6.— As figure 2 but for the [N II] λ6584/[O II] $\lambda\lambda$3727,29 against the [O III] λ5007/[O II] $\lambda\lambda$3727,29 ratio used by Dopita et al. (2000). This is an excellent diagnostic of both metallicity and of stellar age. Note that the [O III] λ5007/[O II] $\lambda\lambda$3727,29 ratio is sensitive to *both* age and metallicity. This diagram suggests that most H II regions are observed in the age range 1–3 Myr.

are quenched, while the lower threshold energy [N II] λ6584 continue to be excited. For this reason as well, the [N II]/[O II] line ratio falls with increasing abundance.

The decrease in electron temperature with metallicity also affects the [O III] λ5007/[O II] $\lambda\lambda$3727,29 ratio as well. By itself, this would induce an increase in the [O III]/[O II] ratio with metallicity. However, this is more than offset by two factors. Firstly, the mean effective temperature of the exciting stars falls with metallicity, and secondly, the mean ionization parameter is itself a decreasing function of metallicity. Both of these lead to a net decrease in the [O III]/[O II] line ratio with metallicity. Nonetheless, the [O III]/[O II] line ratio remains a sensitive indicator of the ionization parameter, which is strongly age dependent. Therefore, a plot of [N II] λ6584/[O II] $\lambda\lambda$3727,29 against the [O III] λ5007/[O II] $\lambda\lambda$3727,29 ratio should separate stellar age from stellar abundance. This is illustrated in figure 6.

It is clear that the [O III] λ5007/[O II] $\lambda\lambda$3727,29 ratio is an excellent diagnostic of both stellar age and of stellar abundance. According to the theoretical tracks, all the observed H II regions have ages between 0 and roughly 4 Myr, with most lying in the age range 1–3 Myr. The division into abundance bins by use of the [N II] λ6584/[O II] $\lambda\lambda$3727,29 is very clean. Provided that the calibration is correct, then the abundance can be obtained using only the [N II]/[O II] ratio to a precision of roughly 0.15 dex.

The [O III] λ5007Hβ line ratio can be substituted for the [O III]/[O II] ratio, since both are sensitive to ionization parameter and therefore to the age of the cluster. However, the separation into age classes is not so sharp using this ratio, as can be seen in figure 7. Furthermore, we have seen in figure 4 that the models tend to systematically underestimate the [O III] λ5007/Hβ ratio, so therefore it follows the age of the H II regions using this diagnostic is also likely to be an underestimate of the true age.

The third figure from Dopita et al. (2000) which utilizes the [N II] λ6584/[O II] $\lambda\lambda$3727,29 ratio is that which plots this ratio against the [O III] λ5007/ [N II] λ6584 ratio. The [O III] $\lambda\lambda$4959,5007/ [N II] $\lambda\lambda$6548,84 ratio was first proposed by Alloin et al. (1979) as a more convenient abundance diagnostic, which is very nearly equivalent to the one we are using here. The observations and theoretical curves on this diagnostic are shown in figure 8.

Pettini & Pagel (2004) have argued that the [O III] λ5007/ [N II] λ6584 is of itself a sensitive abundance indicator suitable to be used in the analysis of abundances in high-redshift galaxies. This, however, is a little too simplistic. Because the [O III]/[N II] ratio is strongly dependent upon the excitation of the nebula, it is also sensitive to both the ionization parameter, as shown by Dopita et al. (2000) and to the age of the cluster of exciting stars. These sensitivities are as great as the sensitivity to abundance alone. Nonetheless, the [N II] λ6584/[O II] $\lambda\lambda$3727,29 *vs.* [O III] λ5007/ [N II] λ6584 diagnostic plot has great

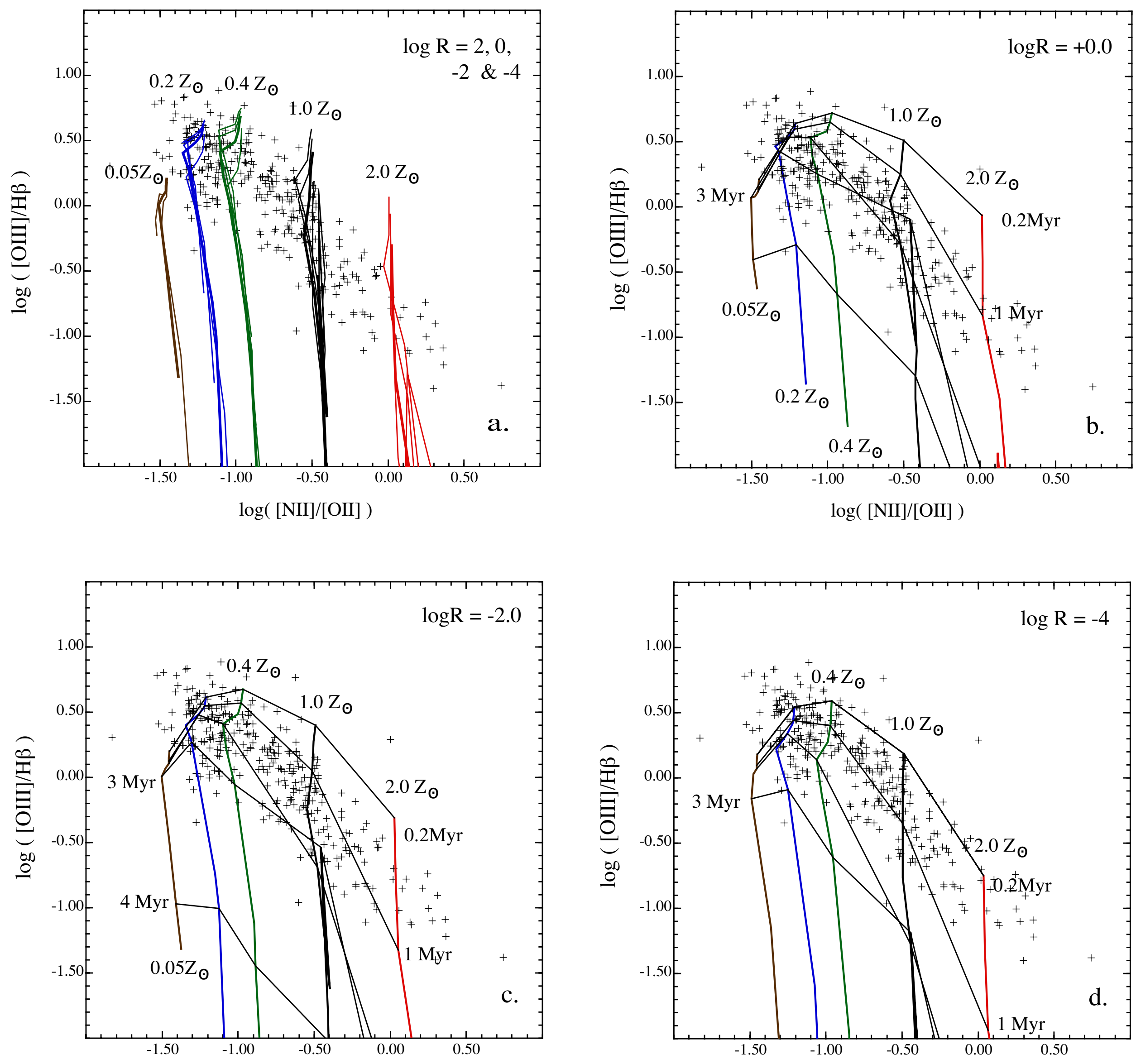

Fig. 7.— As figure 2 but for the [N II] λ6584/[O II] $\lambda\lambda$3727,29 against the [O III] λ5007/Hβ ratio, as used by Dopita et al. (2000). This is also a good diagnostic of both metallicity and of stellar age. Given that the models tend to underestimate the [O III] λ5007/Hβ ratio, the age of the H II regions using this diagnostic is also likely to be an underestimate.

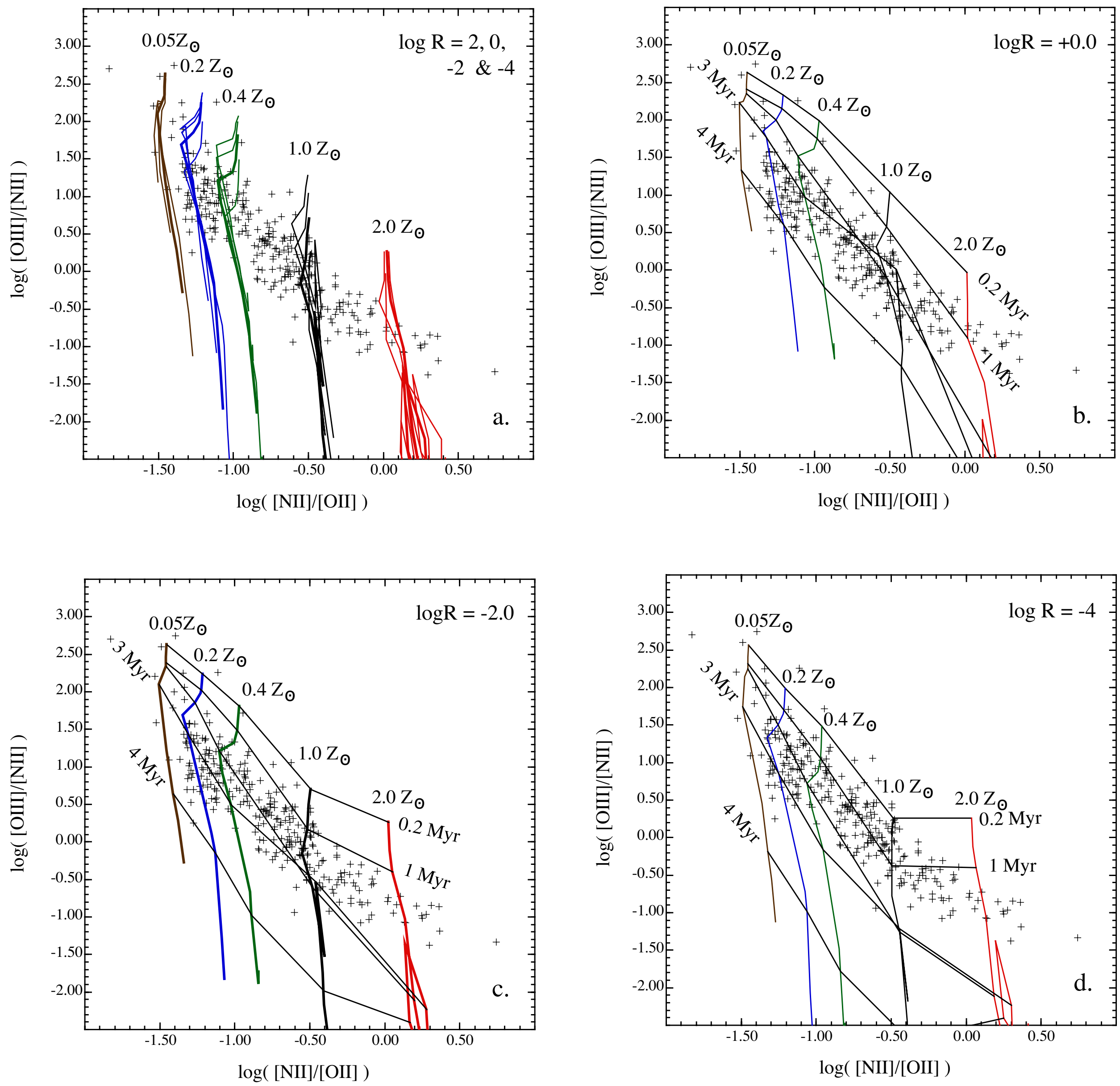

Fig. 8.— As figure 2 but for the [N II] λ6584/[O II] $\lambda\lambda$3727,29 against the abundance-sensitive [O III] λ5007/ [N II] λ6584 ratio, as proposed by Alloin et al. (1979). Although the [O III]/[N II] ratio is indeed sensitive to abundance, it is also very sensitive to ionization parameter as shown by Dopita et al. (2000) and therefore to stellar age. This diagram suggests that most H II regions are observed in the age range 1–3 Myr, in good agreement with age estimate obtained by figure 6.

utility in separating abundance from cluster age, and the results that it gives are in broad agreement with figure 6. From these two plots we can conclude that most H II regions are observed in the age range 1–3 Myr with little sensitivity of this age range with abundance.

This is in full accord with expectations. As shown in Paper II, after an age of 3 Myr, the absolute luminosity of H II regions in the recombination lines drops sharply, and due to the expansion of the H II region, the surface brightness drops even more rapidly. Both of these militate strongly against the observation of old H II regions in extragalactic studies. Furthermore, very young H II regions tend to be dust obscured since they are still embedded in their placental molecular cloud complex. Such H II regions will not be bright at optical wavelengths. In Paper II we estimated the molecular cloud dissipation timescale for the molecular clouds to be about 1 Myr using the particular example of M17. The molecular cloud dissipation timescale was introduced in Paper I, and is the characteristic timescale τ for the H II region to emerge from its compact or ultra-compact configuration, and is a measure of the solid angle (as by at the exciting stars) which is intercepted by molecular clouds; $\Omega(t)/4\pi = \exp[-t/\tau]$. Clearly, the relative dearth of young H II regions beween 0.2 and 1.0 Myr, evident in figures 6 and 8, is consistent with $\tau \sim 1$ Myr.

In conclusion then, the [N II] λ6584/[O II] $\lambda\lambda$3727,29 ratio *vs.* the [O III] λ5007/ [N II] λ6584 is a good diagnostic of both metallicity and age of the exciting cluster. The [O III] λ5007/ [N II] λ6584 ratio can only be used by itself as an abundance indicator to the degree to which we can assume a (fairly restricted) characteristic age for the exciting clusters. Statistically, this may be valid, but the results of its use in single galaxies should be treated with caution.

3.1.5. [N II]/Hα vs [S II]/Hα

Because they are very close to each other in wavelength, and because we have seen that [N II] is very sensitive to abundance, [N II] λ6584/Hα *vs.* [S II] $\lambda\lambda$7617,31/Hα offers some hope as an abundance diagnostic. This has recently been investigated by Moustakas & Kennicutt (2005), who was interested to find out whether his integrated spectra of galaxies were different from single H II regions when plotted in this way. We would expect to find such a difference in principle, because integrated spectra do not discriminate against the emission from old H II regions in the manner described in the previous section. The results of our modelling is shown in figure 9.

Note how the integrated spectra on figure 9 are concentrated along the right-hand side of the region defined by the observations of single H II regions. This reflects the fact that

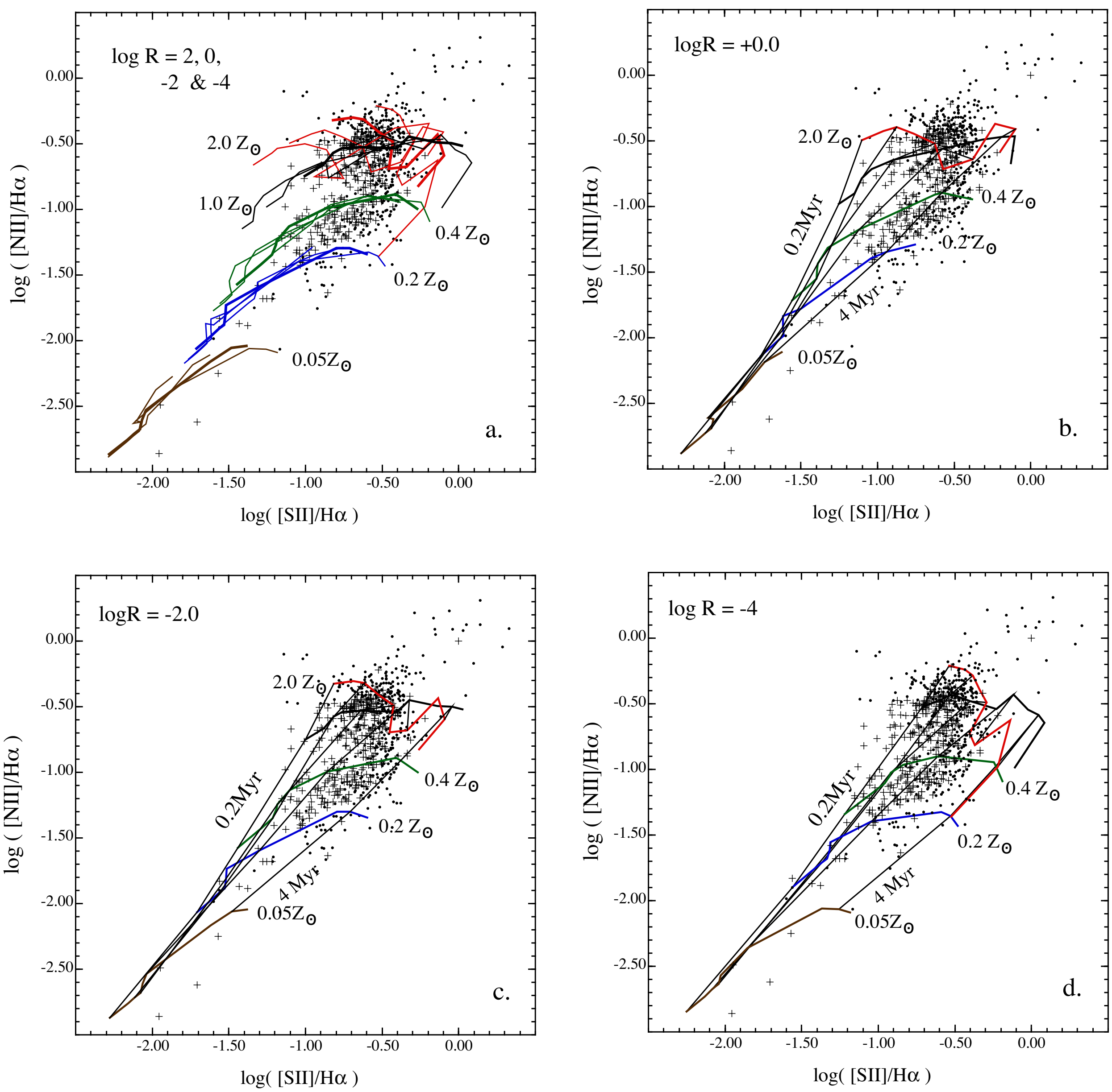

Fig. 9.— As figure 2 but for the [N II] λ6584/Hα *vs.* [S II] $\lambda\lambda$7617,31/Hα diagnostic line ratios. As in Figure 2 the data for individual H II regions are shown as crosses, and the integrated spectra from Moustakas & Kennicutt (2005) are shown as points. Because these are both ratios of lines in the red portion of the spectrum, and because N is partially a secondary element, this diagnostic turns out to be a good abundance diagnostic for $Z/Z_{\odot} <$ 1.0. The older and more diffuse H II regions are located close to the right hand boundary of the observation points. This gas can be identified with the warm ionized medium (WIM) in galaxies.

integrated galaxy spectra include the diffuse component of the ISM, even when this has a low surface brightness, because the total flux in the diffuse component may be an appreciable portion of the total emission.

In Paper II, we found that the diffuse component due to old, evolved, large and faint H II regions could amount to 20–30% of the total Hα emission, and suggested that this could be identified with the Diffuse Ionized Medium (DIM) which is almost ubiquitously seen in disk galaxies (Hoopes, Waterbos & Greenwalt 1996; Martin 1997; Wang, Heckman & Lehnert 1998, 1999). This is usually refereed to as the "Reynolds Layer" in the context of our own Galaxy; see a recent review by Reynolds (2004). In the past, the excitation of the DIM has been usually ascribed to leakage of ionizing photons from young H II regions. However, the emission from large, faint, low pressure and evolved H II regions might provide a better explanation.

In figure 9, old H II regions with metallicities $Z/Z_{\odot} > 1.0$ reach up to line ratios of [S II] $\lambda\lambda$7617,31/H$\alpha \sim 1$ and [N II] $\lambda\lambda$6548,84/H$\alpha \sim 2/3$, which is certainly consistent with the observed line ratios of much of the DIM. However, in our Galaxy, line ratios even greater than this are seen. To explain these, we would have to invoke an additional heating mechanism, such as shocks, or a harder EUV field possibly produced by old ex-nuclei of Planetary Nebulae, which are sufficiently numerous to produce an appreciable EUV field out of the plane of the Galaxy.

3.2. Infrared Line Diagnostics

The ISO satellite first demonstrated the utility of mid-IR line diagnostics in the analysis of H II region spectra. For normal galactic H II regions, Giveon et al. (2002) obtained extensive ISO spectroscopy, as did Peeters et al. (2002) in the context of Ultra-Compact (UC) H II regions. Later, Verma et al. (2003) measured integrated spectra for a number of famous Starburst galaxies. We will use these data here, although we note that both the high-resolution and low-resolution modes of the Infrared Spectrometer (IRS) (Houck et al. 2004) on the *Spitzer Space Observatory* are producing much new and excellent data on both individual H II regions as well as on spectroscopy of whole galaxies.

Within the spectral range of the IRS, line ratio plots that can be constructed are of the excitation: excitation nature. Examples include the [Ne III] 15.5μm / [Ne II] 12.8μm ratio, the [S IV] 10.5μm / [S III] 18.7μm ratio, the [S IV] 10.5μm / [Ar III] 9.0μm ratio, and the [Ne III] 15.5μm / [S III] 18.7μm ratio. Unfortunately, these are of little use in measuring anything other than the hardness of the EUV radiation field. All of the strong lines accessible in this region of the spectrum are produced by $\alpha-$process elements, and therefore the abundance ratios stay approximately constant with abundance. All the lines have low energy thresholds for excitation, and therefore none of them are particularly sensitive to the electron temperature, which varies strongly with abundance. In figure 10 we present only one example to demonstrate how poor these line ratios are as abundance diagnostics when used alone.

In order to form a line ratio that is sensitive to abundance, we need to use a ratio with a Hydrogen or Helium recombination line. Unfortunately, these are faint in the mid-IR. About the best line we have is Brα $\lambda 4.051\mu$m. Alternatively, Pfund$-\alpha$ $\lambda 7.458\mu$m might be useable, although it is often difficult to observe against the PAH features seen at this wavelength. In figure 11 we show one such diagnostic, the [Ne III] 15.5μm / [Ne II] 12.8μm ratio versus the [Ne III] 15.5μm / Brα $\lambda 4.051\mu$m line ratio. This provides a very clean separation between the different abundance sequences.

Note that the observations from Giveon et al. (2002) are consistent with abundances between 2.0 and 0.4 $Z_{\odot}$, and with ages between 0 and 2 Myr. This abundance range is exactly what we would expect to find for Galactic H II regions over the range of Galactocentric radii observed by him. It is interesting that the ages are lower than those derived for H II regions at optical wavelengths. This is consistent with the selection criteria for IR-bright, compact H II regions. This selects for young H II regions. Additionaly, the use of mid-IR wavelengths allow the H II region emission to be seen almost unimpeded by the surrounding molecular material, so the molecular cloud dissipation timescale is not a relevant parameter here.

4. Integrated Spectra

The diagnostics for the previous section were designed to derive parameters for single H II regions. However, what we seek to do is a spectral synthesis by taking recombination line flux averaged spectra along an evolutionary track of an H II region with given parameters. This then reduces the number of free parameters to two; $Z/Z_{\odot}$ and $\log R$. The observations can then be used to constrain the values $\log R$, allowing the extragalactic abundance sequence for ensemble averages of evolving H II regions to be derived. This technique opens the way to the accurate study of the metallicity history of the Universe.

On line ratio diagnostics, there is no simple relationship between the ensemble averaged line ratio and the line ratios in the individual H II regions which make up this average. For example, a high ionization line such as [O III] $\lambda 5007$ will be mostly produced in the very youngest H II regions with the highest $R-$values. Low ionization lines such as the

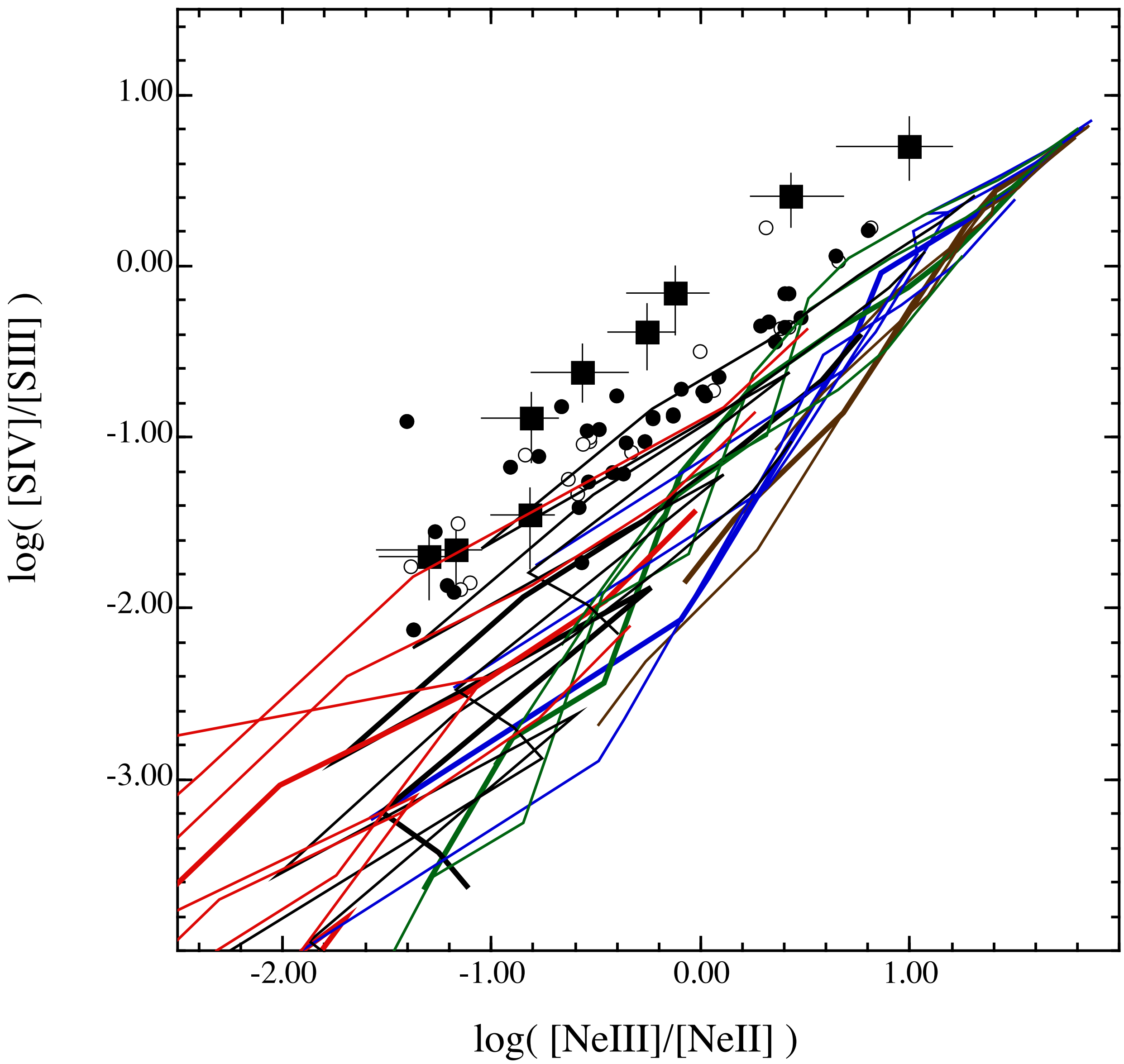

Fig. 10.— The [Ne III] 15.5μm / [Ne II] 12.8μm ratio versus the [S IV] 10.5μm / [S III] 18.7μm ratio. H II regions from Giveon et al. (2002) are plotted as filled circles, UC H II from Peeters et al. (2002) as open circles, and Starburst galaxies from Verma et al. (2003) as filled squares with error bars. The theoretical curves create as superb an example of theoretical spaghetti as anything these authors have seen.

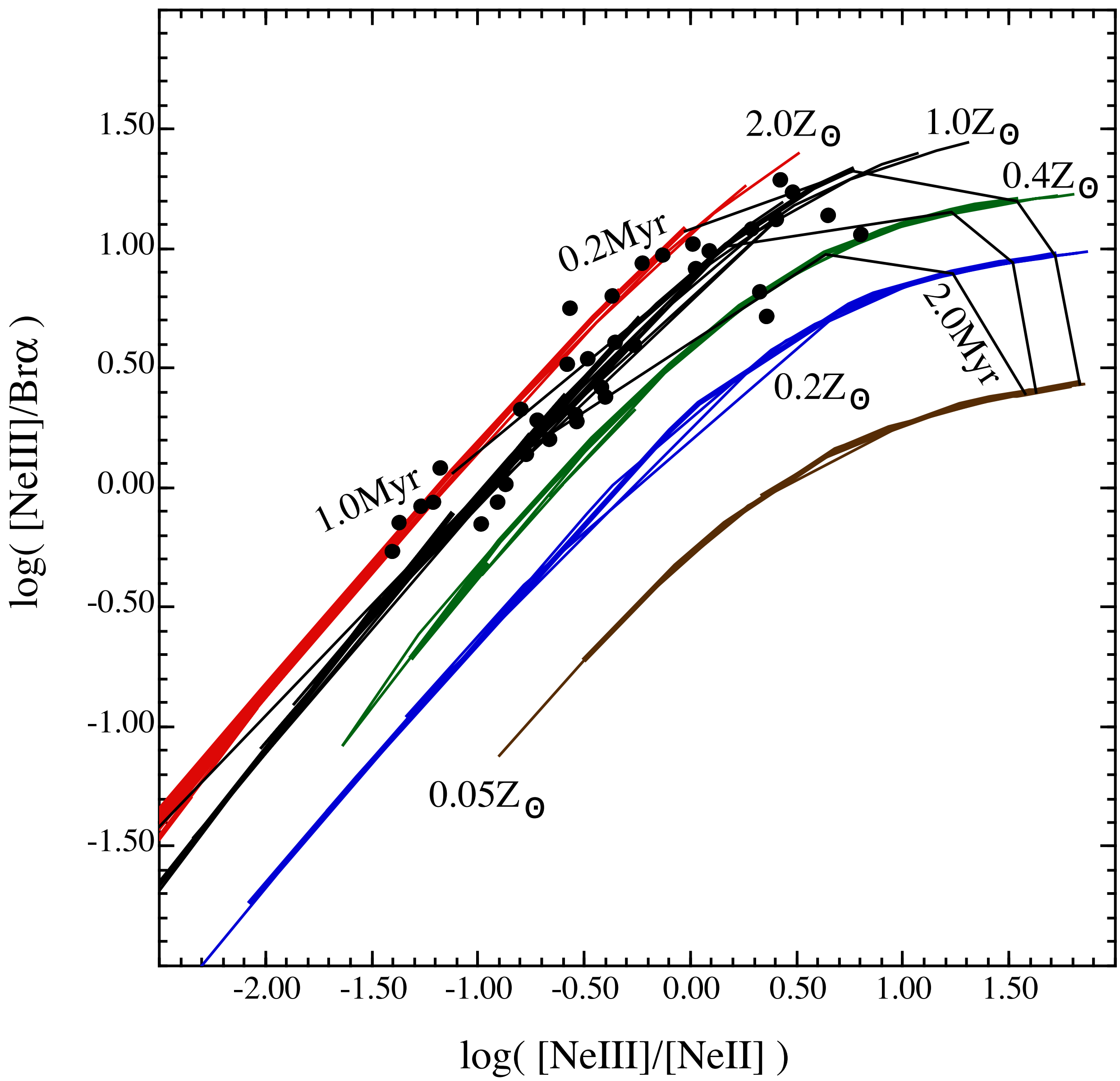

Fig. 11.— The [Ne III] 15.5μm / [Ne II] 12.8μm ratio versus the [Ne III] 15.5μm / Brα λ4.051μm line ratio. H II regions from Giveon et al. (2002) are plotted as filled circles. This diagnostic provides a clean abundance determination which is monotonic over the full abundance range. The isochrones are given for the case $\log R = -2$. This diagram is an infrared analog of fig 4, but is a much cleaner diagnostic because these IR line ratios are very insensitive to the nebular temperature.

[S II] $\lambda\lambda$7617,31 lines will have a much greater weighting from older evolved H II regions with low $R-$values. Indeed, for this line the majority of the line flux may come from regions lying outside the bright H II regions that would be normally selected for observation in studies of individual H II regions - in other words, from regions that form part of the 'warm ionized medium' (WIM).

Given these quite different selection biases, it is interesting to compare line ratio observations of the integrated line fluxes of galaxies with those of individual H II regions. Such a comparison helps us to quantify the importance of the WIM in determining the global line ratio. For this purpose, we have used the observations of individual H II regions listed and used above, and we have drawn our sample of integrated line fluxes of galaxies from the Nearby Field Galaxy Survey (NFGS) (Jansen et al. 2000), and the recent survey by Moustakas & Kennicutt (2005).

In figure 12 we plot the main V&O diagnostic [N II] λ6584/Hα *vs.* [O III] λ5007/Hβ. This should be compared with figure 2. Note that the integrated spectra fit better to the modeled spectra of individual galaxies than do the models of individual H II regions to the data on individual H II regions in figure 2. This is especially apparent at the low abundance end (where most observations are of relatively nearby dwarf irregular galaxies such as NGC6822, IC1613, IIZw40 and the like). This suggests that the observations of these low-abundance H II regions may be affected by aperture effects. This would be caused by observers picking out bright high-excitation sub-regions of the H II region from their long-slit spectra for analysis, rather than observing across the whole H II region to obtain an integrated spectrum of it. This would preferentially enhance the [O III] λ5007/Hβ ratio while at the same time depressing the [N II] λ6584/Hα ratio, moving the observed point in line ratio space towards the top and the left.

The fit with the second V&O diagnostic, the [S II] $\lambda\lambda$7617,31/Hα *vs.* [O III] λ5007/Hβ (figure 13) is less convincing. The integrated spectra are displaced to the right on the [S II] $\lambda\lambda$7617,31/Hα ratio compared with the spectra from individual H II regions, showing the importance of the contribution of the more diffuse ionized component. It is interesting to note that most of the highest points in terms of the [O III] λ5007/Hβ ratio are contributed by the Moustakas & Kennicutt (2005) data set. In this respect there are systematic differences between this data set and the NFGS survey. The reason for this is not apparent to us.

In the models, the [N II] $\lambda\lambda$6548,84 are the major coolants in the outer parts of the H II regions. It is possible that the abundance of Nitrogen in the ionized gas is somewhat overestimated (by an underestimate of the depletion, for example), leading to saturation in the [N II] λ6584/Hα ratio, and a reduction in the [S II] $\lambda\lambda$7617,31/Hα ratio.

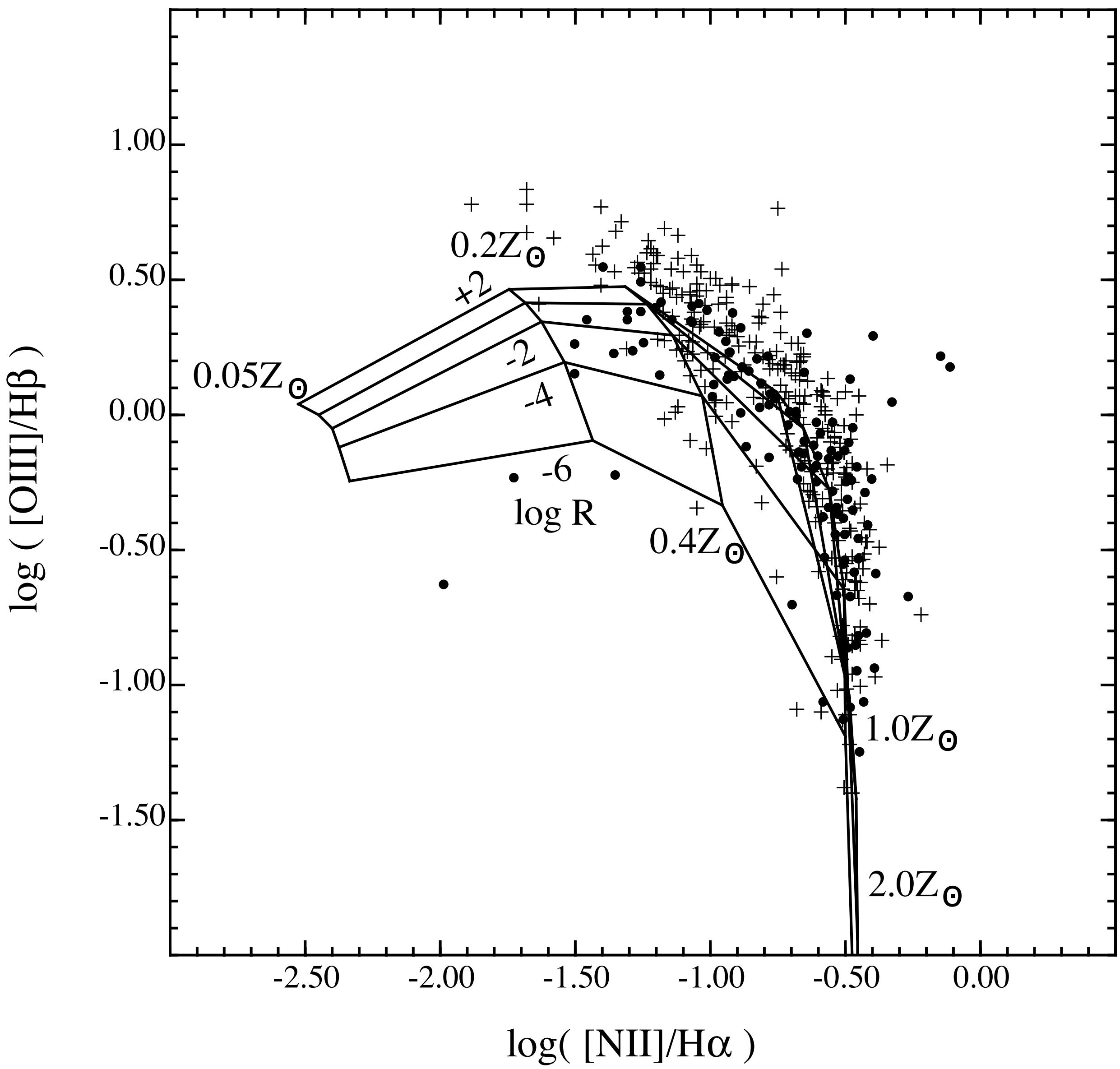

Fig. 12.— The synthesised H II region spectra on the V&O diagnostic [N II] $\lambda6584/\mathrm{H}\alpha$ *vs.* [O III] $\lambda5007/\mathrm{H}\beta$ (c.f. figure 3). The integrated galaxy spectra from the Nearby Field Galaxy Survey (NFGS) (Jansen et al. 2000) are shown as filled circles, while the crosses are for individual H II regions drawn from the sources referenced above. The theory provides an excellent fit to the data, providing that $\log R > -4$. Note the large disparity between the integrated spectra and the observations of individual H II regions at the low abundance end ($Z/Z_{\odot} < 0.4$).

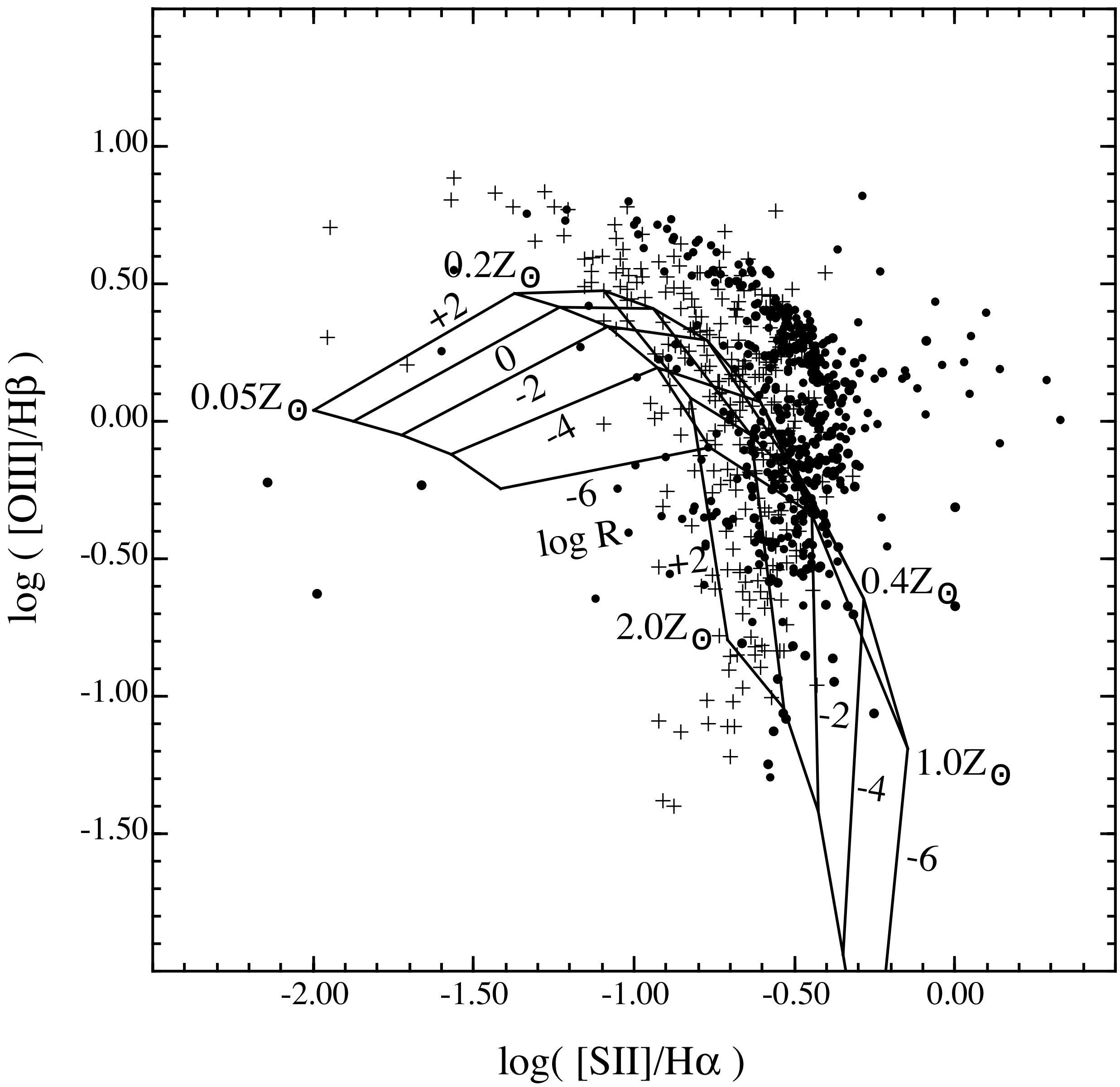

Fig. 13.— The synthesised H II region spectra on the V&O diagnostic [S II] $\lambda\lambda$7617,31/Hα *vs.* [O III] λ5007/Hβ (c.f. figure 4). The integrated galaxy spectra are shown as filled circles, and include both the NFGS data and the data from Moustakas & Kennicutt (2005). Both the [S II] $\lambda\lambda$7617,31and the [O III] λ5007seem to be a little weak in the models compared with the observations.

The problem with the models in reproducing the observed [S II] $\lambda\lambda$7617,31/Hα ratios is systematic. Even with the old *Starburst 99 v2* models, a similar problem was encountered by Dopita et al. (2000). This will be discussed further in the next section.

Turning now to the BPT diagram, the [O III] λ5007/[O II] $\lambda\lambda$3727,29 ratio *vs.* the [O III] λ5007/Hβ ratio (Baldwin, Phillips & Terlevich 1981), which is plotted in figure 14. Once again, the fit between the theory and observation is good, although on this diagnostic the data once again fall somewhat high relative to the theory in the [O III] λ5007/Hβ ratio at the low abundance end $Z/Z_{\odot} < 0.4$. Both figure 12 and figure 14 suggest that the lower abundance bound to the NFGS survey is about $Z/Z_{\odot} < 0.2$. Figure 13 and figure 14 suggest that the upper bound is about $Z/Z_{\odot} \sim 2$.

The first of the Dopita et al. (2000) diagnostics is shown in figure 15. This plots the [N II] λ6584/[O II] $\lambda\lambda$3727,29 ratio against the [O III] λ5007/[O II] $\lambda\lambda$3727,29 ratio, and should be compared with figure 6. There is very little distinction between the distribution of the integrated spectra from the NFGS survey and the observations of individual H II regions on this diagram. Essentially any value of $\log R$ seems to be permitted, although the majority of the points are consistent with a range 0 to -4 in this parameter. This is consistent with what we might have expected, given that the parameters which enter into R $(M_{\rm cl}/(P/k)$ cover at least the range $100 < M_{\rm cl}/M_{\odot} < 10^5$ and $10^4 < P/k < 10^7{\rm cm}^{-3}{\rm K}$.

The abundance range of the NFGS survey suggested by this plot is broader than that given by the V&O or BPT diagnostics, since the theory implies the existence of some galaxies with very low abundances. However, we must beware once again of the observation problems which enter into plots like this. The [N II] λ6584 line and the [O II] $\lambda\lambda$3727,29 lines lie at opposite ends of the spectrum, and so there is a very large reddening correction applied to the data. Generally speaking a standard reddening law is used to do this. In the case of the NFGS survey, for example the Clayton, Cardelli & Mathis (1989) extinction curve was used. However, the foreground dust screen in front of an individual H II region (let alone a whole galaxy) has a complex fractal structure, and rather than using an extinction curve, an attenuation curve should be used instead, see Fischera, Dopita & Sutherland (2003); Fischera & Dopita (2005) and Paper I.

The effect of an attenuation law will be to cause the strengths of lines in the red to be underestimated, while UV lines such as the [O II] $\lambda\lambda$3727,29 lines will be systematically overestimated. These effects will mean that the observations corrected using an extinction law will land systematically too far to the right and too low on this diagram, while on (almost) extinction-free diagnostics such as the V&O plots, the data will plot onto the correct position. If this effect is the cause of the displacement between theory and observation seen in figure 14, this suggests that the [O III] λ5007/[O II] $\lambda\lambda$3727,29 ratio may be systematically

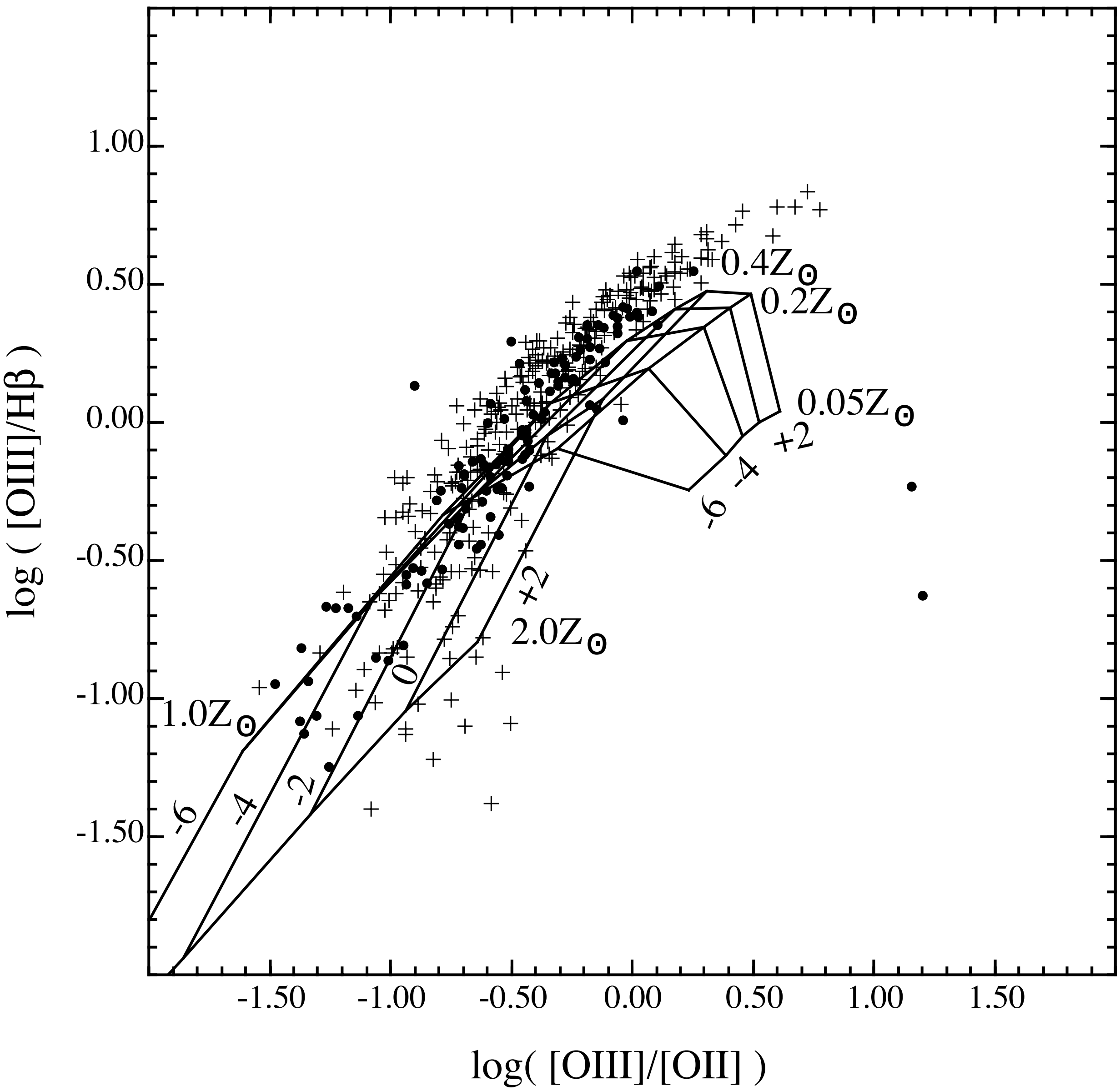

Fig. 14.— As figure 12, but for the BPT diagram, the [O III] λ5007/[O II] $\lambda\lambda$3727,29 ratio vs [O III] λ5007/Hβ . This should be compared with figure 5.

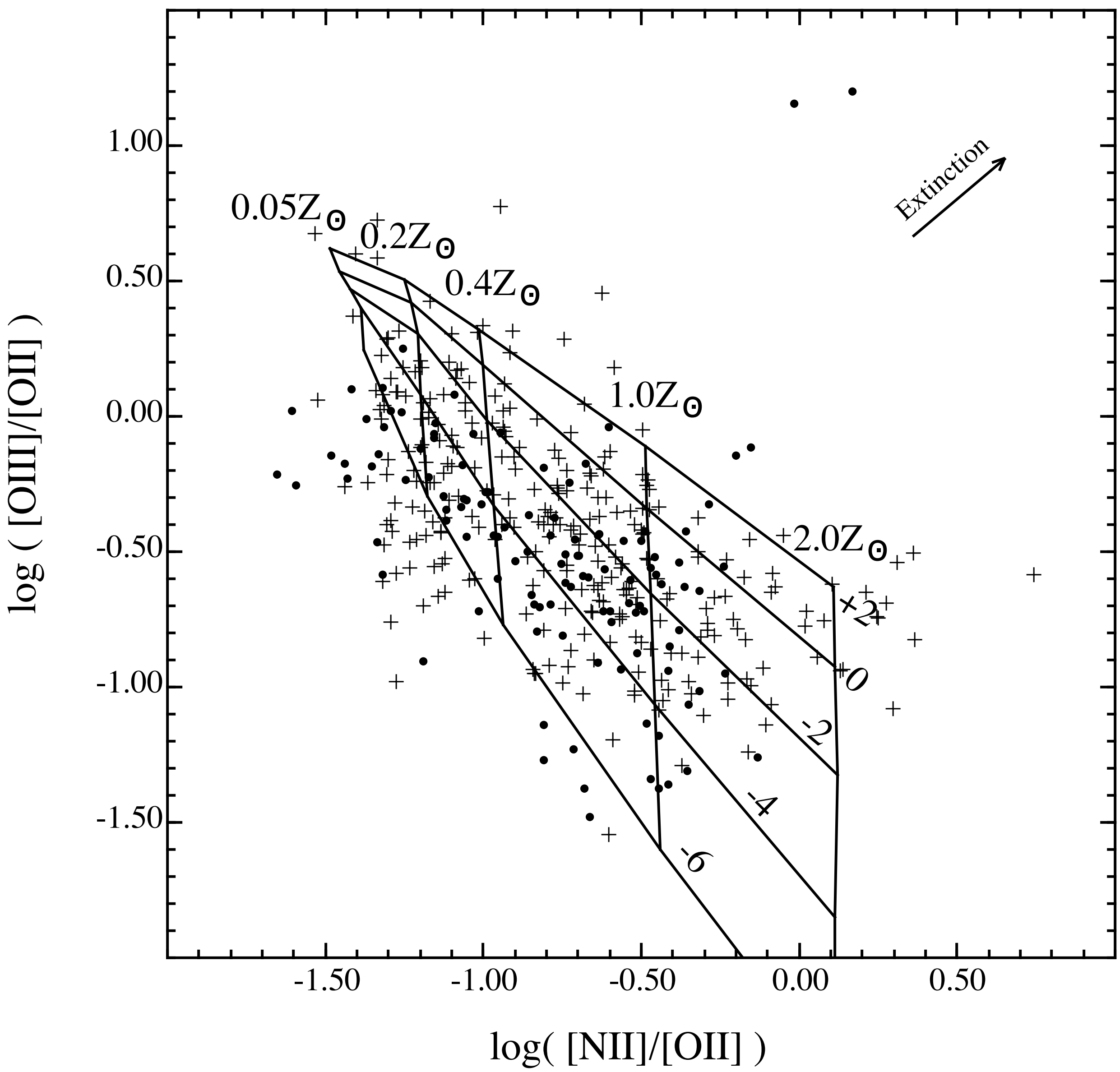

Fig. 15.— As figure 12 but for the [N II] $\lambda6584$/[O II] $\lambda\lambda3727,29$ ratio against the [O III] $\lambda5007$/[O II] $\lambda\lambda3727,29$ ratio used by Dopita et al. (2000). This should be compared with figure 6. This is perhaps the most unambiguous diagnostic for the determination of both metallicity and $\log R$. For the meaning of the arrow marked 'extinction' see the text.

underestimated by $\sim$ 0.3dex. This would imply that the [N II] λ6584/[O II] $\lambda\lambda$3727,29 ratio may be underestimated by a similar amount, since the extinction is determined from the Hα/Hβ ratio which means that the observed [N II] λ6584/[O III] λ5007 ratio must necessarily be correct. The effect of a correction of this magnitude is shown on figure 15 as an arrow marked 'extinction'. With a correction of this magnitude, not only can the lower bound of the abundance in the NFGS survey be reconciled with that given by figure 12 ($Z/Z_{\odot} \sim 0.2$), but also with the upper bound indicated by figure 14 ($Z/Z_{\odot} \sim 2$). The range on $\log R$ would then be 2 to -4.

A systematic overestimate of the [O II] $\lambda\lambda$3727,29 lines would also lead to a systematic overestimate of R_{23}. This may well account for much of the discrepancy between theory and observation in figure 5.

A similar effect is seen in the second of the Dopita et al. (2000) diagnostics is shown in figure 15. This plots the [N II] λ6584/[O II] $\lambda\lambda$3727,29 ratio against the [O III] λ5007/Hβ ratio. Here too we show the effect that a sytematic extinction correction error of 0.3 dex would have on the observations. Once again, they would shift into a range which is consistent with the abundance and R bounds given above.

Finally, we plot the [S II] $\lambda\lambda$7617,31/Hα ratio versus the [N II] λ6584/Hα line ratio in figure 17 (compare with figure 9). This shows, once again, the value of the [N II] λ6584/Hα line ratio as an abundance diagnostic in its own right. It also illistrates, once again, our difficulties with the [S II] $\lambda\lambda$7617,31/Hα ratio, with the observations, particularly the Moustakas & Kennicutt (2005) data set falling to the right of the theoretical curves in this ratio.

5. Discussion & Conclusions

It is clear that these models represent a significant advance in our understanding of the strong line spectra of H II regions. In particular, the models explicitly account for the dynamical evolution of the H II region controlled through the mechanical energy input by both the stellar winds and supernova explosions. We find that two factors largely control the excitation of the young H II regions, both of these dependent on the chemical abundance. These are:

- The effective temperature of the exciting stars, which increases with decreasing metallicity, and
- The control of the ionization parameter by the stellar winds in the expanding H II regions. This was shown in Paper II to increase with decreasing metallicity

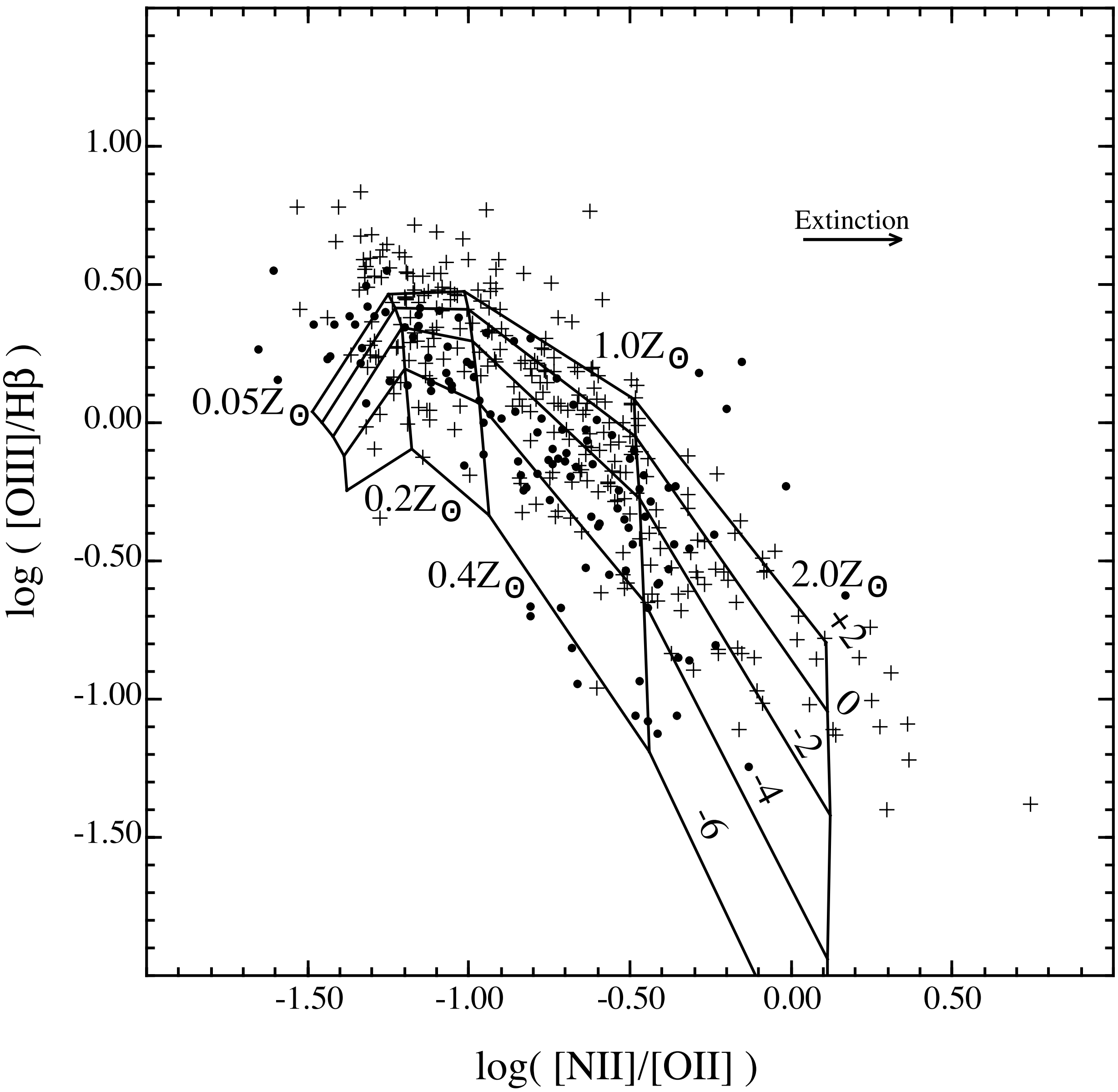

Fig. 16.— As figure 12, but for the [N II] λ6584/[O II] $\lambda\lambda$3727,29 ratio against the [O III] λ5007/Hβ ratio used by Dopita et al. (2000). This should be compared with figure 7. This is a good diagnostic for the determination of both metallicity and $\log R$. The observations and the theory would give consistent answers in all integral spectrum diagnostics if a systematic correction is made to the observations of the magnitude illustrated by the arrow marked 'extinction' in this and the previous figure (see text).

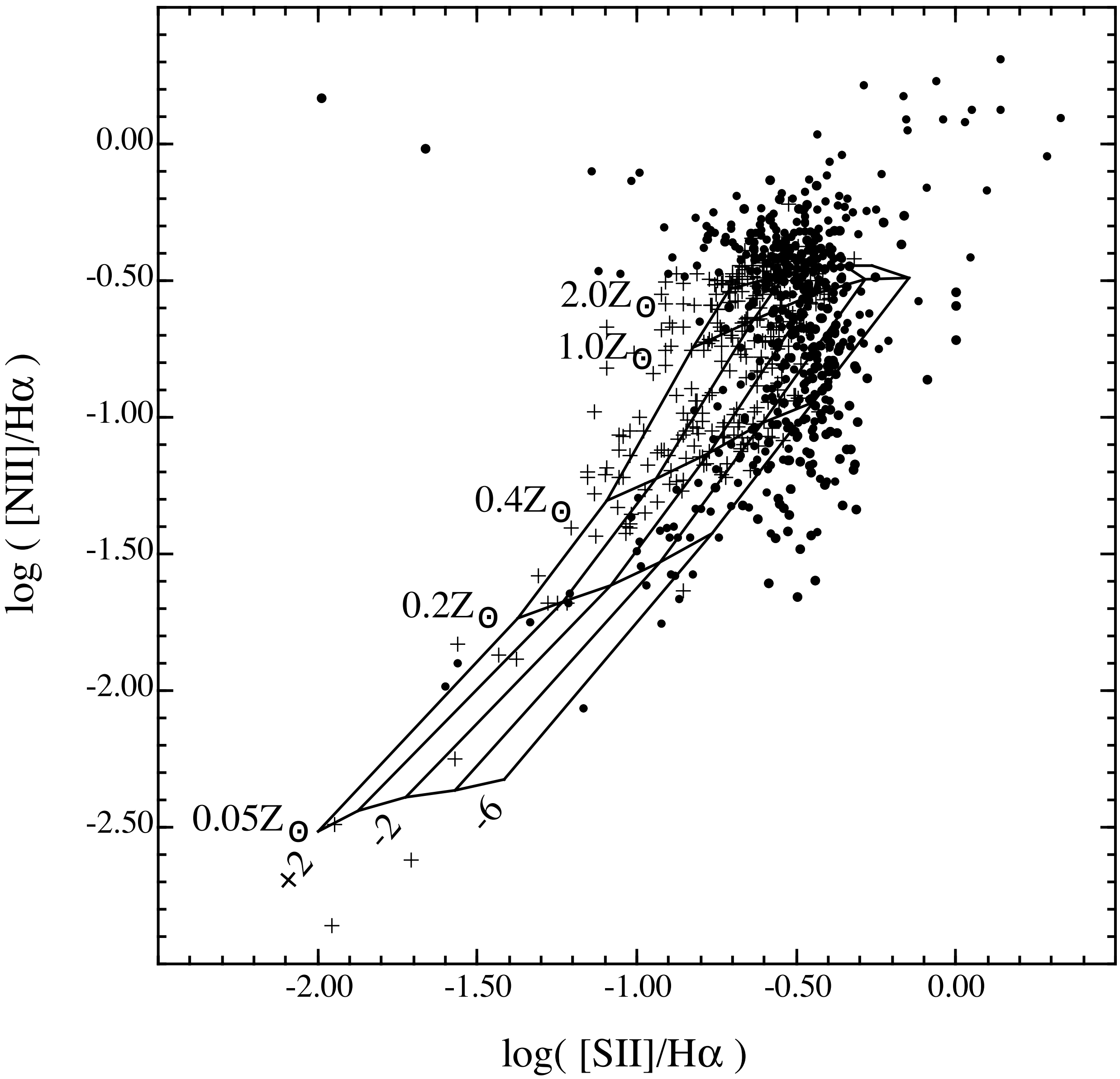

Fig. 17.— As figure 12, but for the [N II] λ6584/Hα ratio against the [S II] $\lambda\lambda$7617,31/Hα ratio. This should be compared with figure 9. This once again illustrates our problems in modelling the [S II] line strengths.

Since both of these effects operate to increase the excitation of low abundance H II regions, we therefore find an abundance dependent excitation, which much improves the fit of the theory compared to models in which the ionization parameter is treated as a free variable. In our models the ionization parameter is replaced by the R parameter, the ratio of the cluster mass in solar masses to the pressure in the ISM; P/k (cm^{-3}K). This parameter is used because all models with a given R have a unique relationship between their instantaneous ionization parameter and time. This allows us to construct evolutionary tracks for ensembles of H II regions.

With increasing age, the ionization parameter falls almost monotonically, and the H II region fades after reaching its maximum brightness in Hα after 1-2 Myr. The presence of Wolf-Rayet stars after about 3.5 Myr causes the effective temperature of the cluster to briefly increase. This increases the excitation for a short time, causing the 3 Myr and the 4 Myr isochrones to cross over each other on diagnostic plots for the cases of high metallicity ($Z/Z_{\odot} > 0.5$, approximately).

In this paper, we have identified a number of useful diagnostics for deriving the abundance and either the age, in the case of isolated H II regions, or the R parameter, in the case of integrated spectra of galaxies. Our diagnostics for the integrated spectra are the first which explicitly take into account the fact that when we observe a whole galaxy, we are observing an ensemble average of H II regions of all ages, sizes and central cluster masses. The simplification we have been able to make by using the R parameter has rendered this problem tractable to a more simple analysis other than treating each H II region separately, and adding the whole lot together at the end.

In comparing the models to the observational data we have identified some potential problems with the way that observations have been made and analyzed. In particular,

- long-slit observations do not integrate over the whole of an H II region, particularly in the case of observations of nearby, low metallicity dwarf irregular galaxies. By picking out the brightest regions of such H II regions, we bias the data towards the high-excitation regions and the spectrum is not representative of the whole H II region and,

- the use of a reddening correction using an extinction curve, rather than an attenuation curve (which is appropriate for spatially extended objects) will cause the line intensities of UV lines to be systematically overestimated, biasing the strong line diagnostics which use the [O II] $\lambda\lambda$3727,29 Å lines.

This second effect would reveal itself in the spectro-photometry as a failure to reproduce the correct intensities of the higher members of the Balmer Series, such as Hδ or Hϵ, and so should be quite easy to check for in observational data sets. Such an effect would also influence the measurement of the strength of the [O III] λ4363Å line, again causing it to be overestimated. This could be part of the reason for the long-standing discrepancy between the abundances derived from the strong lines and those obtained from measurements of the electron temperature using ratios such as [O III] λ4363Å/[O III] λ5007 , see Bresolin, Garnett & Kennicutt (2004) for a recent discussion. We expect that the major part of the discrepancy will turn out to be caused by temperature fluctuations. However, this could be easily corrected for by assuming the Case B recombination line ratio between Hβ and Hγ, and measuring the forbidden line strengths relative to the nearest Balmer lines in the spectrum.

There is clearly a need for integral field spectrophotometry on extragalactic H II regions to allow efficient construction of integrated spectra. This would also help in the removal of stellar flux from the spectrum. Such observations would help to remove the remaining discrepancies between theory and observation which is important in the use of theoretical integral spectra in the analysis of the chemical evolution history of the early Universe.

The models too have their deficiencies. In general, all the low ionization species are predicted weaker than observed. These include the [O I] λ6300, the [S II] $\lambda\lambda$7617,31, and the [O II] $\lambda\lambda$3727,29, although these lines are probably affected by the reddening corrections made to the observations.

What could enhance the [S II] $\lambda\lambda$7617,31/Hα ratio or the [O I] λ6300/Hα ratio? First, both the the O I and the S II ion are very much more sensitive than the N II ion to the diffuse radiation field in H II regions. They are therefore much enhanced in the vicinity of ionization fronts, and in shadow regions behind elephant trunk features, which are obscured from direct stellar radiation and illuminated only by the diffuse nebular radiation field. Second, both are much enhanced in shock regions. Indeed high [S II]/Hα ratios are used as a means of identifying supernova remnants either embedded in H II regions or in the ISM at large, and [O I]/Hα ratios reach 0.5 or higher in shock-excited regions. Neither of these effects are taken into account in the models.

In addition, the O I ion is locked by charge-exchange reactions to the concentration of H I. Furthermore, the collision strength of [O I] λ6300 increases with electron temperature. To produce a high [O I] λ6300/Hα ratio in a purely photoionized region requires the presence of a hard radiation field. This could originate either as a thermal soft X-ray continuum from the shocked bubble of stellar wind material, or it could simply be an indication of a hotter sub-component in the global stellar radiation field.

If the radiation field produced by *Starburst 99 v5.* is too soft, this could be rectified in at least three ways, First, by the use of a flatter IMF in the upper mass ranges ($M/M_{odot} > 10$). This could be possible because observationally we have very few constraints other than by use of the excitation of H II regions. Second, by adding another stellar component such as mass-exchange massive binaries to the stellar synthesis.

A third - and quite likely possibility is that the EUV spectrum of the massive stars used in *Starburst 99 v5.* may be in error. With previous versions of *Starburst 99* based on the *CoStar* models (Shaerer & de Koter 1997), the EUV spectrum was, rather, too hard. However, Morisset et al. (2004) has demonstrated that the theoretical number of ionizing photons emitted by the central star and the shape of the ionizing spectrum is highly dependent upon the atmospheric model used. At one extreme are the *CoStar* models, at the the other extreme are found the 'classical' *Kurucz* (Kurucz 1991, 1994) plane-parallel LTE line blanketed models used in *Starburts99 v5.*. The Kurucz models display the softest EUV spectra and the lowest photoionising flux, and are restricted to $\log g = 3.0$ for the models with higher effective temperature, $T_{\rm eff}$. In between these extremes are found three sets of models with fairly similar photoinising flux predictions (Morisset et al. 2004), the *TLUSTY* models of Lanz & Hubeny (2003a,b), the *WM-Basic* models of Pauldrach, Hoffman, & Lennon (2001) and the *CMFGEN* models Hillier & Miller (1998). Of these, the *TLUSTY* models are plane-parallel hydrostatic, while the other two are spherical dynamic atmospheres. All of this offers plenty of potential for error in the estimation of the the hardness of the EUV spectrum for a given cluster mass and metallicity.

Given that the [O III] λ5007/Hβ ratio of the models also appears to be on the low side, we believe that an increase in the stellar effective temperature, either by a flattening of the IMF or by some other means offers the best chance to more properly match the theory with the observations. The models are too weak in their forbidden line strengths overall. The Stoy (1933) method (Pottasch & Preite-Martinez 1983) of deriving the effective temperature of the exciting stars relies upon measuring the total flux cooling lines (which is a measure of the mean energy per photoionization) to a recombination line (which counts the number of photoionizations). Thus, if we want to increase the absolute strengths of the forbidden lines, we have to increase the stellar effective temperature. This increase would also strongly increase the [O I] λ6300/Hα ratio by both increasing the extent of the partially-ionized zonr and by increasing the electron temperature within it.

A niggling uncertainty with the modeling is the mis-match between the *Starburst 99 v5* abundance set and the abundance set given in table 1. The *Starburst 99 v5* has to rely on the older stellar evolution models which use the old value of the solar abundances. In an attempt to quantify this effect, we ran a test model with a $0.4Z_{\odot}$ spectral synthesis cluster model from *Starburst 99 v5* embedded in a nebula with $1.0Z_{\odot}$ (using the abundances given in table 1). This made surprisingly little difference, changing critical line ratios by 0.1 dex or less, except for the [O I] λ6300/Hα ratio, which increased by 34%. We therefore conclude that the results presented in this paper are reasonably secure against any future adjustment of stellar atmospheric abundances.

Dopita acknowledges the support of both the Australian National University and the Australian Research Council (ARC) through his ARC Australian Federation Fellowship. Dopita, Sutherland & Fishera acknowledge financial support of ARC Discovery project grant DP0208445. Kewley acknowledges a Hubble Fellowship. The work by van Breugel was performed under the auspices of the U.S. Department of Energy and Lawrence Livermore National Laboratory under contract No. W-7405-Eng-48.

This work by van Breugel was performed under the auspices of the U. S. Department of Energy by University of California, Lawrence Livermore National Laboratory under contract W-7405-Eng-48.

Here we give a summary of the strong line flux ratios with respect to Hβ as computed in the photoionization models. The line identifications, the ionic species and the wavelengths of each line listed in the electronic version of this paper are given in Table 2.

Table 1. Solar metallicity ($Z_{\odot}$) and depletion factors (D).

Element	log($Z_{\odot}$)	log(D)
H	0.00	0.00
He	-1.01	0.00
C	-3.59	-0.15
N	-4.22	-0.23
O	-3.34	-0.21
Ne	-3.91	0.00
Mg	-4.47	-1.08
Si	-4.49	-0.81
S	-4.79	-0.08
Ar	-5.20	0.00
Ca	-5.64	-2.52
Fe	-4.55	-1.31

Table 2. Line ID and Wavelength list

Line ID #	λ (Å)	Ion	Line ID #	λ (Å)	Ion
01	H I	1215.7	27	[S II]	6716.3
02	C III]	1909.1	28	[S II]	6730.7
03	C III]	1911.2	29	[Ar III]	7135.7
04	[C II]	2325.2	30	[Ar III]	7751.0
05	Mg II	2797.9	31	[S III]	9069.3
06	[O II]	3726.0	32	H I	10049.4
07	[O II]	3728.7	33	H I	10049.4
08	H I	3797.9	34	He I	10830.0
09	H I	3835.4	35	He I	10833.0
10	[Ne III]	3868.7	36	H I	10938.1
11	He I	3888.6	37	H I	12818.1
12	H I	3889.1	38	H I	18751.0
13	[Ne III]	3967.4	39	H I	26252.0
14	H I	3970.1	40	H I	40512.0
15	H I	4104.7	41	[Ar II]	69832.8
16	H I	4340.5	42	[Ar III]	89892.5
17	He I	4471.5	43	[S IV]	105221
18	H I	4861.3	44	[Ne II]	128115
19	[O III]	4958.8	45	[Ne III]	155513
20	[O III]	5006.8	46	[S III]	186821
21	He I	5875.6	47	[S III]	336366
22	[O I]	6300.2	48	[Si II]	347941
23	[N II]	6548.0	49	[O III]	517972
24	H I	6562.8	50	[N III]	573845
25	[N II]	6583.3	51	[O III]	883017
26	He I	6678.2	..	..	..

In the electronic version of the paper, separate tables are given for each of the abundances computed; 0.05, 0.2, 0.4, 1.0 and 2.0 $Z_{\odot}$, and in each of these tables, line fluxes with respect to H$\beta = 1.0$ are given for each of the 51 lines listed in Table 2. These spectral line intensities are given for each value of $\log R$ computed; +2, 0, -2, -4 and -6. The quantity R is that defined in the text of the paper:

$$R = \left[\frac{M_{\rm cl}}{M_{\odot}}\right]\left[\frac{P/k}{10^4{\rm cm}^{-3}{\rm K}}\right] \qquad (1)$$

Each of the five electronic tables (Tables 3 through 7) follows the same format. A short extract is given of the first of these (Table 3) to illustrate the format and content followed by all.

REFERENCES

Alloin, D. et al. 1979, A&A, 78, 200

Anders, E. & Grevesse, N. 1989, Geochim. & Cosmochim. Acta 53, 197

Asplund, M., Grevesse, N. & Sauval, A. J. 2005, in *Cosmic Abundances as Records of Stellar Evolution*, eds T. G. Barnes & F. N. Bash, ASP Conf. Ser. 336,

Baldwin, J. A., Phillips, M. M., & Terlevich, R. 1981, PASP, 93, 5

Bresolin, F., Garnett, D. R., & Kennicutt, R. C. Jr. 2004, ApJ, 615, 228

Castor, J., McCray, R. & Weaver, R. 1975, ApJ, 200, L107

Cardelli, J. A., Clayton, G. C. & Mathis, J. S. 1989, ApJ, 345, 245

Dennefeld, M. & Stasinska, G. 1983, A&A, 118, 234

Dopita, M. A. & Evans, I. N. 1986, ApJ, 307, 431

Dopita, M. A., Kewley, L. J., Heisler, C. A., & Sutherland, R. S. 2000, ApJ, 542, 224

Dopita, M. A., Groves, B. A., Sutherland, R. S., Binette, L. & Cecil, G. 2002, ApJ, 572, 753

Dopita, M. A., et al. 2005, ApJ 619, 755 (Paper I)

Dopita, M. A., et al. 2006, in press (Paper II)

Edmunds, M. G., & Pagel, B. E., J. 1984, MNRAS, 211, 507

Table 3. Fluxes in HII region models with respect to Hβ for the 0.05 times solar abundance set.

log R Line ID	λ (Å)	F(0.1Myr)	F(0.5Myr)	F(1.0Myr)	F(1.5Myr)	F(2.0Myr)	F(2.5Myr)	F(3.0Myr)	F(3.5Myr)	F(4
+2										
01	1.216E+03	3.584E+01	3.509E+01	3.477E+01	3.460E+01	3.439E+01	3.191E+01	3.122E+01	3.330E+01	3.09
02	1.909E+03	2.070E-01	1.775E-01	1.666E-01	1.616E-01	1.568E-01	1.426E-01	1.456E-01	1.164E-01	7.8
03	1.911E+03	1.358E-01	1.162E-01	1.090E-01	1.057E-01	1.026E-01	9.324E-02	9.530E-02	7.632E-02	5.1
04	2.325E+03	6.546E-03	7.732E-03	8.224E-03	8.454E-03	8.621E-03	1.037E-02	1.071E-02	1.156E-02	1.7
..	..	..	..	..	..	..	..	..	..	
..	..	..	..	..	..	..	..	..	..	
51	8.830E+05	1.393E-01	1.743E-01	1.790E-01	1.804E-01	1.809E-01	1.748E-01	1.690E-01	1.337E-01	1.0
+0										
01	1.216E+03	3.581E+01	3.509E+01	.478E+01	3.461E+01	3.440E+01	3.191E+01	3.138E+01	3.422E+01	3.18
02	1.909E+03	2.063E-01	1.768E-01	1.656E-01	1.603E-01	1.556E-01	1.411E-01	1.341E-01	6.801E-02	4.0
..	..	..	..	..	..	..	..	..	..	
..	..	..	..	..	..	..	..	..	..	
-2										
..	..	..	..	..	..	..	..	..	..	
..	..	..	..	..	..	..	..	..	..	
-4										
..	..	..	..	..	..	..	..	..	..	
-6										
..	..	..	..	..	..	..	..	..	..	

Fischera, J., Dopita, M. A, & Sutherland, R. S. 2003, ApJ, 599, 21

Fischera, J., & Dopita, M. A 2005, ApJ, 619, 340

Garnett et al. 1999, ApJ, 513, 168

Giveon, U., Sternberg, A., Lutz, D., Feuchtgruber, H. & Pauldrach, A. W., A. 2002, ApJ, 556, 880

Groves, B. A., Dopita, M. A., & Sutherland, R. S. ApJS, 153, 9

Hoopes, C. G., Waterbos, R. A. M., & Greenwalt, B. E., AJ, 112, 1429

Houck, J. R. et al. 2004, ApJS, 154, 18

Hillier, D. J. & Miller, D. L. 1998, ApJ, 496, 407

Jansen, R. A., Franx, M., Fabricant, D., & Caldwell, N. 2000a, ApJS, 126, 271

Kennicutt, R. C. Jr. & Garnett, D. R. 1996, ApJ, 456, 504

Kewley, L. J.; Heisler, C. A.; Dopita, M. A., & Lumsden, S. 2001a, ApJS, 132, 37

Kewley, L. J, Geller, M. J, Jansen, R. A. & Dopita, M. 2002a, AJ, 124, 3135

Kewley, L. & Kobulnicky, H.A. 2005, in Starbursts - From 30 Doradus to Lyman Break Galaxies, eds, R. de Grijs & R.M. González Deggado, ASSL Conf Ser. (Springer: Berlin), 329, 303

Kimura, H., Mann, I. & Jessberger, E. K. 2003, ApJ, 582, 846

, Kobulnicky, H. A., Kennicutt, R. C., & Pizagno, J. L. 1999, ApJ, 514, 544

, Kobulnicky, H. A., & Zaritsky, D. 1999, ApJ, 511, 120

Kurucz, R. L. 1991, in "Stellar Atmospheres: Beyond Classical Models", eds L. Crivellari, I. Hubeny, & D. Hummer, NATO ASI Ser. C, 341, 441

Kurucz, R. L. 1992, in IAU Symp. 149, "The Stellar Populations of Galaxies", ed. B. Barbuy & A. Renzini (Dordrecht:Kluwer), 225

Kurucz, R. L. 1994, "Solar Abundance Model Atmospheres for 0, 1, 2, 4 and 8 km/s, Kurucz CD-ROM no. 19, Cambridge, Mass:SAO, 1994, 19

Lanz, T., & Hubeny, I. 2003a, ApJS, 146, 417

Lanz , T., & Hubeny, I. 2003b, ApJS, 147, 225 (erratum)

Lejeune, Th., Cuisinier, F. & Buser, R. 1997, A&AS, 125, 229

Leitherer, C., Gruenwald, R. & Schmutz, W. 1992, in *Physics of Nearby Galaxies* ed. T. X. Thuan, C. Balkowski, & J. T. T. Van, Éditions Frontiéres, 257

Leitherer, C., Schaerer, D., Goldader, J. D., Delgado, R. M. González, R. C., Kune, D. F., de Mello, Duília F., Devost, D., & Heckman, T. M. 1999, ApJS, 123, 3

McCall, M. L., Rybski, P. M., & Shields, G. A. 1985, ApJS, 57, 1

McGaugh, S. S. 1991, ApJ, 380, 140

Martin, C. L. 1997, 491, 561

Miller, G. E. & Scalo, J. M. 1979, ApJS, 41, 513

Morisset, C., Schaerer, D., Bouret, J.-C. & Martins, F. 2004, A&A, 415, 577

Moustakas, J. & Kennicutt, R. C. Jr. 2005, asto-ph/0511731

Moustakas, J. & Kennicutt, R. C. Jr. 2006, ApJS, in press.

Oey, M. S., Shields, J. C., Dopita, M. A. & Smith, R. C. 2000, RevMexAA, 12, 77

Oey, M. S., Parker, J. S., Mikles, V. J. & Zhang, X. 2003, AJ, 126, 2137

Oey, M. S., King, N. L. & Parker, J. S., 2004, AJ, 127, 1632

Pagel, B. E. J. et al 1979, MNRAS, 189, 95

Pagel, B. E. J., Edmunds, M. G., & Smith, G. 1980, MNRAS, 193, 219

Pagel, B. E. J., Simonson, E. A., Terlevich, R. J. & Edmunds, M. G. 1992, MNRAS, 255, 325

Pauldrach, A. W. A., Hoffman, T. L., & Lennon, M. 2001, A&A, 374, 161

Peeters, E., et al. 2002, A&A, 381, 571

Pettini, M. & Pagel, B. E. J. 2004, MNRAS, 348, 59

Pilyugin, L. S. 2000, A&A, 362, 325

Pottasch, A. S., & Preite-Martinez, A. 1983, A&A, 302, 69

Reynolds, R. J., 2004, Advances in Space Research, 34, 27

Roy, J.-R. & Walsh J. R. 1997, MNRAS, 288, 715

Russell, S. C. & Dopita, M.A. 1992, ApJ, 384, 508

Shaerer, D. & de Koter, A. 1997, ApJ, 211, 722

Skillman, E. D., Kennicutt, R. C., & Hodge, P. W. 1989, ApJ, 347, 875

Smith, L. J., Norris, R. P. F., & Crowther, P. A. 2002, MNRAS, 337, 1309

Steidel, C C., Giavalisco, M., Pettini, M., Dickinson, M. & Adelberger, K. L. 1996, ApJ, 462, 17

Stoy, R. H. 1933, MNRAS, 93, 588

Sutherland, R. S. & Dopita, M. A. 1993, ApJS, 88, 253

Torres-Peimbert, S., Peimbert, M., & Fierro, J. 1989, ApJ, 345, 186

van Zee, L. *et al.* 1998, AJ, 116, 2805

Veilleux, S. & Osterbrock, D. E., 1987, ApJS, 63, 295

Verma, A., Lutz, D., Sturm, E., Sternberg, A., Genzel, R. & Vacca, W. 2003, A&A, 403, 829

Wang, J., Heckman, T. M., & Lehnert, M. D. 1998, ApJ, 509, 93

Wang, J., Heckman, T. M., & Lehnert, M. D. 1999, ApJ, 515, 97

Walsh J. R. & Roy, J.-R. 1997, MNRAS, 288, 726

Zaritsky, D., Kennicutt, R. C., & Huchra, J. P. 1994, ApJ, 420, 87